AKADEMIA GÓRNICZO-HUTNICZA IM. STANISŁAWA STASZICA W KRAKOWIE

FACULTY OF ELECTRICAL ENGINEERING, AUTOMATICS, COMPUTER SCIENCE AND BIOMEDICAL ENGINEERING

DEPARTMENT of Power Electronics and Energy Control Systems

Bachelor Thesis

Identification of mathematical model parameters of induction motor

Author: Montserrat Caso Fernández
Field of study: Industrial Technology Engineering
Advisor: Jaroslaw Kozik

Kraków, 2016

AKADEMIA GÓRNICZO-HUTNICZA IM. STANISŁAWA STASZICA W KRAKOWIE

WYDZIA ELEKTROTECHNIKI, AUTOMATYKI, INFORMATYKI I INYNIERII BIOMEDYCZNEJ

KATEDRA Energoelektroniki i Automatyki Systemów Przetwarzania Energii

Praca dyplomowa inynierska

Identyfikacja parametrów modelu matematycznego silnika indukcyjnego

Autor:	Montserrat Caso Fernandez
Kierunek studiów:	Industrial Technology Engineering
Opiekun pracy:	Jaroslaw Kozik

Kraków, 2016

Uprzedzony o odpowiedzialności karnej na podstawie art. 115 ust. 1 i 2 ustawy z dnia 4 lutego 1994 r. o prawie autorskim i prawach pokrewnych (t.j. Dz.U. z 2006 r. Nr 90, poz. 631 z późn. zm.): "Kto przywłaszcza sobie autorstwo albo wprowadza w błąd co do autorstwa całości lub części cudzego utworu albo artystycznego wykonania, podlega grzywnie, karze ograniczenia wolności albo pozbawienia wolności do lat 3. Tej samej karze podlega, kto rozpowszechnia bez podania nazwiska lub pseudonimu twórcy cudzy utwór w wersji oryginalnej albo w postaci opracowania, artystyczne wykonanie albo publicznie zniekształca taki utwór, artystyczne wykonanie, fonogram, wideogram lub nadanie., a także uprzedzony o odpowiedzialności dyscyplinarnej na podstawie art. 211 ust. 1 ustawy z dnia 27 lipca 2005 r. Prawo o szkolnictwie wyższym (t.j. Dz. U. z 2012 r. poz. 572, z późn. zm.) "Za naruszenie przepisów obowiązujących w uczelni oraz za czyny uchybiające godności studenta student ponosi odpowiedzialność dyscyplinarną przed komisją dyscyplinarną albo przed sądem koleżeńskim samorządu studenckiego, zwanym dalej" sądem koleżeńskim, oświadczam, że niniejszą pracę dyplomową wykonałem(-am) osobiście i samodzielnie i że nie korzystałem(-am) ze źródeł innych niż wymienione w pracy.

Table of Contents

List of Figures

Nomenclature

N_s, N_1	Synchronous speed, rpm
f_1	Stator frequency, Hz
f_2	Rotor frequency, Hz
N_2	Rotor speed, rpm
X	Reactance, Ω
s	Induction motor slip
s_{syn}	Induction motor slip at synchronous speed
s_{nom}	Induction motor slip at nominal speed
s_{max}	Induction motor slip at maximum speed
s_sc	Induction motor slip in short-circuit test
f	Frequency, Hz
f_{nom}	Nominal frequency, Hz
n	Number of revolutions per second
p	Number of cycles per revolution (pair of poles)
$\vec{e}$	Electromagnetic force vector, V
l	Length of the conductor immersed in the magnetic field, m
$\vec{v}$	Relative speed vector, m/s
$\vec{\beta}$	Magnetic induction vector, T
θ	Angle between the conductor and the perpendicular direction of the movement , °
$\vec{I}$	Current flowing in the conductor vector, A
$\overrightarrow{F_{me}}$	Mechanical force vector, N
P_input	Input power, W
P_output	Output power, W
$P_{electrical}$	Electrical power, W
$P_{mechanical}$	Mechanical power, W
η	Efficiency
P_{Joule}	Joule losses, W
P_{Cu}	Copper losses, W
P_{Cu1}	Copper losses in the first-stator winding, W
P_{Cu2}	Copper losses in the second-rotor winding, W
P_{Fe}	Iron losses, W
P_{Fe1}	Iron losses in the stator, W
P_{Fe2}	Iron losses in the rotor, W
P_{me}	Mechanical losses due to the friction in the rotating shaft, W
V	Voltage drop, V
I	Current flowing, A
R	Resistance in the circuit, Ω
P_{MH}	Iron losses due to magnetic hysteresis, W
P_{EC}	Iron losses due to eddy currents, W
K_{MH}	Hysteresis constant dependent on material
K_{EC}	Eddy currents constant dependent on material and dimensions
α	Hysteresis constant dependent on material and dimensions
W_{Fe}	Magnetic circuit weight, N
$\hat{\beta}$	Maximum value of magnetic induction, T
U_{nom}	Nominal voltage, V
P_{Fenom}	Nominal iron losses, W

P_{frict}	Friction losses, W
P_{vent}	Self-ventilation losses, W
$K_{frict}, \alpha_{frict}$	Mechanical constants
n_{turn}	Rotating speed
T_{em}	Electromagnetic torque, Nm
T_{dyn}	Dynamic torque, Nm
T_{me}	Mechanical torque, Nm
T_{syn}	Synchronous electromagnetic torque, Nm
T_{max}	Maximum electromagnetic torque, Nm
T_N	Nominal or rated electromagnetic torque, Nm
T_B	Starting or breakaway electromagnetic torque, Nm
T_M	Motor electromagnetic torque, Nm
T_a	Acceleration electromagnetic torque, Nm
T_{frict}	Friction torque, Nm
T_{useful}	Useful torque, Nm
T_{load}, T_L	Load electromagnetic torque, Nm
W_1, W_2	Wattmeters used during the trials, they measured power, W
$N_{2Faulty}$	Rotor speed in Faulty
N_{20}	Rotor speed in no load test
N_{2synch}	Synchronous speed
N_{2sc}	Rotor speed in short-circuit test
U_{1N}	Nominal voltage in the stator, V
U_{2N}	Nominal voltage in the rotor, V
U_L	Line voltage, V
U_p	Phase voltage, V
$\overrightarrow{I_{1N}}$	Nominal current vector in the stator, A
$\overrightarrow{I_{2N}}$	Nominal current vector in the rotor, A
I_L	Line current, A
I_p	Phase current, A
U_{10}	Voltage in the stator windings in no load test, V
U_{10p}	Phase voltage in the stator windings in no load test, V
U_{1sc}	Voltage in the stator windings in short-circuit test, V
U_{1scp}	Phase voltage in the stator windings in short-circuit test, V
U_{20}	Voltage in the rotor in no load test, V
U_{20p}	Phase voltage in the rotor in no load test, V
U'_{20p}	Phase voltage in the rotor in no load test reduced to the stator, V
I_{10}	Current in the stator windings in no load test, A
I_{10p}	Phase current in the stator windings in no load test, A
I_{1sc}	Current in the stator windings in short-circuit test, A
I_{1scp}	Phase current in the stator windings in short-circuit test, A
I_{1Fe0p}	Current flowing through the iron resistance of the stator, A
$I_{1\mu 0p}$	Current flowing through the iron reactance of the stator, A
I_{20}	Current in the rotor in no load test, A
I_{20p}	Phase current in the rotor in no load test, A
I'_{20p}	Phase current in the rotor in no load test reduced to the stator, V
I_{2sc}	Current in the rotor in short-circuit test, A
I_{2scp}	Phase current in the rotor in short-circuit test, A
I'_{2scp}	Phase current in the rotor in short-circuit test reduced to the stator, A

R_1	Stator resistance , Ω
X_1	Stator reactance , Ω
R_2	Rotor resistance, Ω
X_2	Rotor reactance, Ω
R'_2	Rotor resistance reduced to the stator, Ω
X'_2	Rotor reactance reduced to the stator, Ω
R_{Fe}	Iron resistance, Ω
X_μ	Iron reactance, Ω
Z_{sc}	Short-circuit impedance, Ω
R_{sc}	Short-circuit resistance, Ω
X_{sc}	Short-circuit reactance, Ω
R_c	Mechanical resistance, Ω
R'_c	Mechanical resistance reduced to the stator, Ω
φ_0	No load power factor
φ_{sc}	Short-circuit power factor
P_0	Losses in no load test, W
P_{Fe0}	Iron losses in no load test, W
P_{sc}	Losses in short-circuit test, W
P_N	Nominal losses, W
P_{cunom}	Nominal copper losses, W
d	d axis quantity
q	q axis quantity
r	Rotor quantity
st	Stator quantity
l	Leakage quantity
m	Magnetizing quantity
ω	Reference frame angular velocity
ω_r	Electrical angular velocity
φ	Magnetic flux
φ_{qst}	Stator q magnetic flux
φ_{dst}	Stator d magnetic flux
φ'_{qr}	Rotor q magnetic flux reduced to the stator
φ'_{dr}	Rotor d magnetic flux reduced to the stator
L	Magnetic inductance
L_{st}	Stator inductance
L'_r	Rotor inductance reduced to the stator
L_m	Mutual inductance
L_{lst}	Leakage stator inductance
L'_{lr}	Leakage rotor inductance

Acknowledgements

I would like to thank my advisor Jaroslaw Kozik and the rest of people I have met in the laboratories for helping me and giving me advices every time I needed them during the last few months. I would also like to thank my coordinators Janusz Prazuch and Luis Felipe Verdeja González for giving me this opportunity, and the rest of the jury for reading this text. Finally, my sincere gratitude also goes to my family, thank you very much for giving me the chance to keep discovering the world this way.

Montserrat Caso Fernández

Preface

I Introducción

Las máquinas de inducción desempeñan un papel significativo en una gran mayoría de aplicaciones en la actualidad. En el caso concreto de los motores de inducción, sirven de instrumento transformando energía eléctrica en movimiento. No cabe duda que sin este importante avance científico, el mundo que conocemos sería diametralmente diferente. Incluso en el área de estudio del control de velocidad, donde no han sido los más utilizados, están siendo introducidos hoy en día gracias a los inversores de frecuencia variable que verifican su eficiencia. Dada su relevancia, este estudio es un trabajo experimental que persigue el objetivo de destacar su uso, investigar el porqué de su óptima respuesta e implementar un modelo matemático que pueda ser considerado como una simplificación de la realidad, alcanzando rigurosos resultados.

En vista de lo anteriormente expuesto, el objetivo fundamental de esta tesis es dar a conocer el proceso de desarrollo de un modelo matemático que se asemeje al funcionamiento de un motor real a pesar de las simplificaciones incluídas en el mismo. Este estudio, además, proporciona análisis y comparación de resultados explicando sus causas. Con esta finalidad, se han realizado diferentes ensayos conocidos para identificar los parámetros del modelo. Estos parámetros se integran en el modelo como variables de entrada (input values) haciendo que la investigación pueda desarrollarse.

En cuanto al modelo matemático, las siguientes páginas explican ampliamente las simplificaciones propias de este modelo y las transformaciones realizadas a los valores de entrada con el fin de reducir su complejidad tanto en el diseño como en el proceso de simulación.

Con respecto a las medidas relizadas, todas las pérdidas de energía han sido tenidas en cuenta y la mayoría de las señales han sido filtradas debido a la existencia de otras señales de similares frecuencias durante la realización de estos ensayos. Estas señales externas pueden afectar los resultados obtenidos de nuestra investigación, por tanto, durante todo el análisis se ha valorado la posiblilidad de imprecisiones y fallos debido a las mismas.

Para concluir, este estudio comparativo podría cambiar la forma en la que estos motores han sido estudiados hasta nuestros días, consiguiendo una mayor frecuencia en el estudio de los mismos y un avance mucho más rápido y efectivo.

II Máquinas de inducción

La siguiente sección relata el fundamento teórico de las máquinas de inducción, centrándose en su historia, áreas de uso y estructura.

A Información General

El propósito de esta sección es evaluar la relevancia que tienen las máquinas de inducción y dar un breve repaso a su historia.

i Popularidad y áreas de uso

El motor de inducción puede ser considerado una de las invenciones más importantes de la humanidad, por su simplicidad y alta fiabilidad. Un tercio de la electricidad mundial generada es tranformada en energía mecánica en estos motores. Los motores de induccíon son máquinas de arranque automático y robustas en su construcción. A diferencia de los motores DC, no tienen commutadores, lo que elimina todos los problemas relacionados con posibles descargas eléctricas. Por ello, necesitan un mantenimiento menos frecuente, siendo por tanto más económicos. Por los argumentos expuestos, estos motores están muy bien adaptados, no solo para aplicaciones industriales de alta potencia: máquinas de conducción, bombas, ventiladores, compresores, transportadores, ascensores; sino también para multitud de tareas rutinarias. Los motores de inducción continuan dominando el campo de aplicaciones de velocidad fija, y actualmente están siendo introducidos en el área de estudio del control de velocidad gracias a los inversores de frecuencia variable, resultando esto en nuevas aplicaciones como vehículos eléctricos e híbridos.

ii Historia

La invención del motor de inducción es el resultado de numerosos descubrimientos físicos y modelos previos. Durante los pasados siglos, destacados científicos trabajaron en el desarrollo de mejoras en el campo electromágnetico.

Los dos avances más significativos durante este proceso son el motor de inducción de dos fases desarrollado por Nikola Tesla en 1887, conocido por ser el primero en pensar en un sistema de voltaje multifase, y el motor de tres fases diseñado por Dolivo-Dobrowolsky en 1889. Dolivo-Dobrowsky desarrolló tanto el motor de jaula de ardilla como el motor de rotor bobinado, siendo por ello considerado el pionero del sistema trifásico. A lo largo del siglo pasado, se han realizado muchas mejoras en este campo. Siemens, General Electrics, al igual que otras pequeas firmas, continúan desarrollando motores más pequeños y ligeros manteniendo las mismas prestaciones o incluso superándolas.

B Estructura de los motores de inducción

Cada una de las partes de un motor de inducción puede ser dividida en dos grupos: elementos estacionarios o elementos giratorios. La parte estacionaria o el estátor y la parte giratoria denominada rotor.

i Estátor

La corona estatórica está formada por láminas permeables de acero u otro material ferromagnético para evitar las pérdidas por corrientes de Foucault. El material elegido ha de ser un material magnético blando con el propósito de conseguir menos pérdidas por histéresis magnética, ya que estos materiales devuelven la mayoría de la energía almacenada durante el proceso de magnetización. La corona estatórica está ranurada internamente para dejar que el bobinado se sitúe entre las ranuras.

ii Rotor

La corona magnética rotórica está formada por láminas permeables de acero, usando el mismo material que en el estátor. Estas láminas están aisladas eléctricamente unas de otras con el fin de prevenir las indeseadas corrientes de Foucault. La corona magnética rotórica está ranurada exteriormente permitiendo alojarse al bobinado. Dependiendo de la forma constructiva del circuito eléctrico del rotor es posible distringuir dos tipos de motores asíncronos:

Rotor bobinado	**Rotor de jaula de ardilla**
Construcción	
Anillos colectores y escobillas (complicado)	Ausencia de anillos colectores y escobillas (simple)
Bobinado del rotor similar al del estátor	Barras cortocircuitadas en el rotor
Posible añadir resistencias adicionales al rotor	No es posible añadir resistencias adicionales al rotor
Eficiencia	
Altas pérdidas en el cobre	Bajas pérdidas en el cobre (alta eficiencia)
Otras características funcionales	
Mantenimiento frecuente	Menos mantenimiento requerido
Construcción costosa	Construcción más barata
Aplicaciones	
Usados solo en un 10% de aplicaciones industriales	Ampliamente usados
Montacargas, grúas, ascensores etc	Tornos, taladradoras, ventiladores, sopladores y máquinas de impresión etc

Table 1. Diferencias entre rotor bobinado y rotor de jaula de ardilla

iii Estructuras especiales

Ante la imposibilidad de añadir resistencias rotóricas externas a los motores de jaula de ardilla, para mejorar la resistividad del rotor, se deben diseñar unas estructuras rotóricas especiales intrínsecas al rotor que aumenten el momento de arranque. Algunas de estas estructuras especiales son el rotor de doble jaula, el rotor de barra profunda o el rotor de doble jaula de barra profunda que es una combinación de los dos anteriores.

III Principios de operación de los motores de inducción

Esta sección aborda el proceso de generación del campo magnético giratorio y expone las diferentes pérdidas existentes en el modo de operación del motor.

A Producción del campo magnético giratorio

El estátor del motor consiste en la superposición de devanado compensado por un ángulo eléctrico de 120 °. Una vez el arrollamiento primario del estátor está conectado a una fuente de AC de tres fases, cada fase crea una forma de onda del flujo y la combinación de las tres establecen un campo magnético giratorio que gira a la velocidad síncrona. No existe una conexión eléctrica entre el estátor y el rotor, una vez que el campo magnético rotatorio es generado por medio de la combinación de las tres fases de voltaje aplicado este es transmitido al rotor por medio del entrehierro. Las corrientes del rotor, del mismo modo, se inducen a través del entrehierro. El motor de inducción parado se comporta como un transformador cortocircuitado en el bobinado secundario, siendo el bobinado del estátor como el primer bobinado del transformador, y el del rotor como el bobinado secundario del transformador. Al estar cortocircuitado, la corriente interna del rotor depende del voltaje inducido y de su resistencia. Como la velocidad del rotor no puede alcanzar la velocidad de sincronismo, que es la velocidad del campo magnético giratorio, siempre va a existir un deslizamiento s. Si no fuera así no habría velocidad relativa entre el estátor y el rotor, lo que conllevaría a la ausencia de fuerza electromagnética inducida y corriente inducida generando un momento electromagnético.

B Balance energético en motores de inducción

La potencia eléctrica de salida del estátor se convierte en potencia mecánica en el rotor a través del entrehierro. Las transformaciones electromagnéticas y electromecánicas van siempre acompañadas de una serie de pérdidas inevitables que son las siguientes:

- **P**érdidas en el cobre: generadas en los bobinados tanto del estátor como del rotor. La velocidad del rotor en estos motores es menor que la velocidad síncrona, lo que significa que la potencia del rotor es también menor que la potencia transmitida por el campo magnético giratorio. Esta diferencia en potencia se pierde en forma de calor en los bobinados del motor, por lo tanto, estas pérdidas son proporcionalmente dependientes al deslizamiento.

- **P**érdidas en el hierro: generadas en el núcleo del motor, estas pérdidas se producen debido a dos fenómenos magnéticos: histéresis magnética y corrientes de Foucault. Con respecto a su regulación, pueden ser controladas por medio de modificaciones en la frecuencia y en el voltaje. Estas pérdidas no pueden ser nunca mayores a las que se tendrían en condiciones nominales (con frecuencia y voltaje nominal).

- **P**érdidas mecánicas: generadas por la inevitable fricción entre elementos estacionarios y giratorios, entre partes giratorias con el aire, y debido a la autoventilación de la máquina.

IV Cálculo de parámetros y resultados de las mediciones

La máquina usada para la realización de estos experimentos ha sido un motor de inducción de jaula de ardilla con las fases del estátor conectadas en triángulo. El motor está conectado por medio del eje con un generador DC, el cual permite medir la velocidad de rotació de nuestra máquina de inducción.

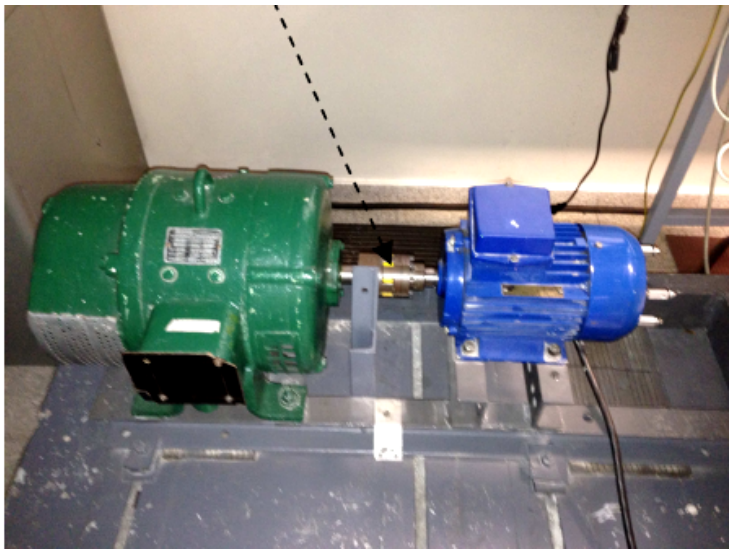

Figure I. Motor de inducción de jaula de ardilla

A Ensayo de vacío

Para esta prueba se ha utilizado el ensayo de vacío con voltajes decrecientes. El estátor es alimentado con voltajes decrecientes desde el voltaje nominal o incluso desde un valor más alto que este, y eliminando cualquier carga del eje (dejando el rotor libre). El valor más bajo de voltaje ha de ser suficiente para mantener la velocidad del rotor similar a la de sincronismo, y así poder suponer las pérdidas mecánicas constantes durante todo el ensayo. Este ensayo se lleva a cabo para obtener los valores de las impedancias de excitación y las pérdidas nominales en el hierro y mecánicas.

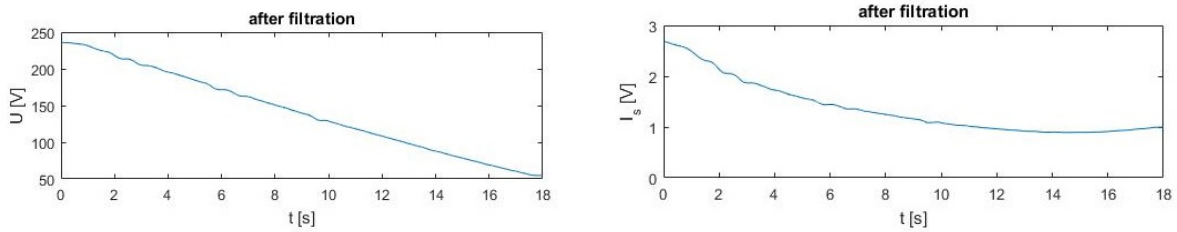

Figure II. Voltaje durante el ensayo de vacío (izquierda) y Corriente durante el ensayo de vacío (derecha)

Se puede apreciar que la corriente decrece a causa del decrecimiento del voltaje suministrado.

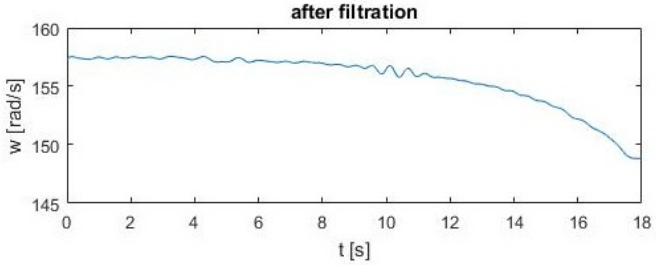

Figure III. Velocidad durante el ensayo de vacío

No cabe duda que el decrecimiento del voltaje y la corriente resultan en un decrecimiento de la velocidad del rotor. Sin embargo, el voltaje disminuye más rápidamente que la velocidad, el cambio en la velocidad requiere más tiempo.

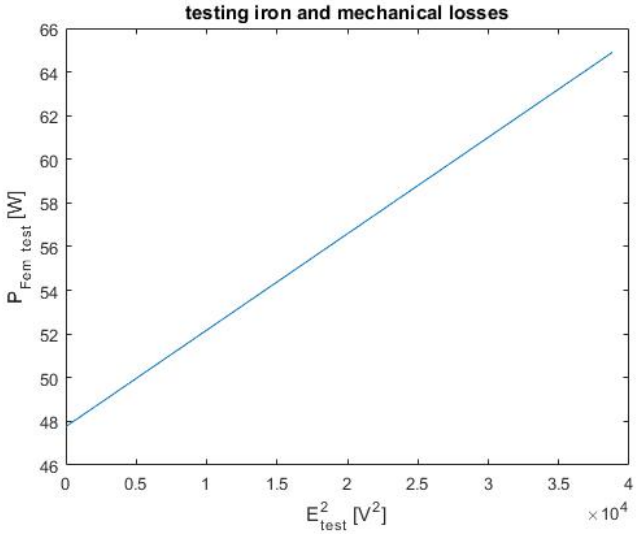

Figure IV. Relación de las pérdidas del hierro y mecánicas con respecto al cuadrado del voltaje inducido

En vista del gráfico anterior, se puede apreciar que a mayor voltaje aplicado, mayores las pérdidas en el hierro (son proporcionales al voltaje) ya que las pérdidas mecánicas durante todo el ensayo se han asumido constantes por lo dicho anteriormente. Por esta razón, la ordenada en el origen de esta recta se refiere a las pérdidas mecánicas.

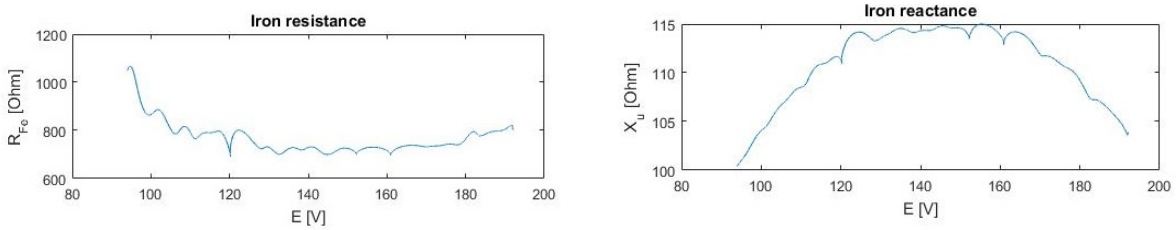

Figure V. Resistencia del hierro (izquierda) y Reactancia del hierro (derecha)

Por la disminución del valor de la resistencia al principio del gráfico, se puede observar que al aumentar el voltaje, aumenta de la misma manera la corriente que fluye por el circuito del rotor haciendo que el valor de la resistencia decrezca. El ligero incremento en el valor de la resistencia al final del gráfico es debido a las altas temperaturas alcanzadas en los cables cuando se aplican voltajes superiores. Sin embargo, este ensayo, al haber sido realizado tomando voltajes decrecientes, el valor de la resistencia aumenta conforme el ensayo se lleva a cabo. En relación a la reactancia, se puede apreciar cómo el núcleo se magnetiza con el aumento en el voltaje, pero este comportamiento tiene un límite. Una vez el núcleo llega a la saturación, este no se puede magnetizar más incluso aplicando volatajes muy superiores, y el valor de la reactancia comienza a disminuir. Esto se observa a partir de aproximadamente 160 V.

B Ensayo de cortocircuito

Este ensayo es realizado alimentando al estátor con corriente nominal e inmobilizando el rotor. El objetivo es determinar las impedancias del bobinado, así como las pérdidas en el cobre.

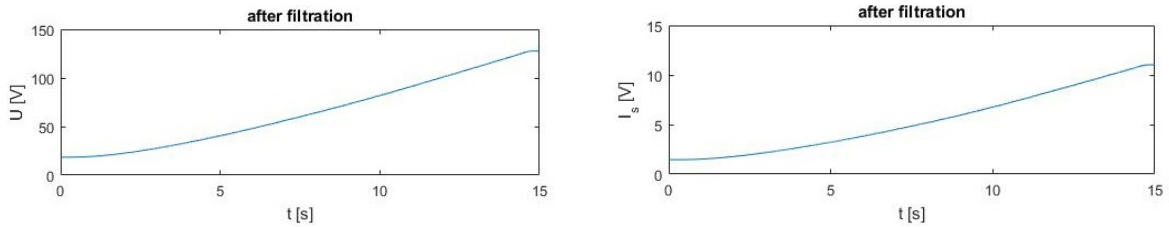

Figure VI. Voltaje durante el ensayo de cortocircuito (izquierda) y Corriente durante el ensayo de cortocircuito (derecha)

Se aumenta el voltaje con el fin de conseguir la corriente nominal necesaria para realizar el ensayo. Como se puede observar por el gráfico de la corriente, no solo se alcanza el valor nominal (6,4 A), sino que se llega a valores mucho más superiores. El incremento en voltaje y corriente conlleva a un incremento en potencia que se traduce en un aumento de pérdidas en el cobre que se liberan en forma de calor en los bobinados de la máquina.

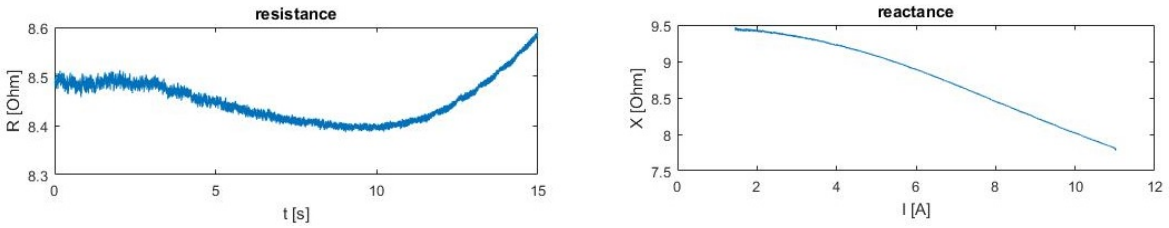

Figure VII. Resistencia del bobinado(izquierda) y Reactancia del bobinado (derecha)

El decrecimiento en el valor de la resistencia en el cobre en este ensayo muestra que el voltaje aumenta más rápidamente que la corriente. A pesar de esta disminución, después de aproximadamente 10 s, se produce un incremento debido a las altas temperaturas soportadas por los cables en este ensayo. Por el contrario, la disminución en el valor de la

reactancia es debido a la permeabilidad del núcleo. A mayor corriente, subsecuentemente la intensidad de campo mágnetico se incrementa y ocurre la saturación del núcleo. Este gráfico muestra que el núcleo se encuentra en saturación, lo que indica que incluso aumentando la corriente, el núcleo no se puede magnetizar más.

C Ensayo de inercia

Este ensayo se realiza teniendo la máquina parada y enrollando una cuerda alrededor del eje con la intención de levantar una carga desde el suelo hasta una altura limitada y luego dejarla caer libremente. El propósito de este ensayo es calcular el momento de inercia del motor estudiado.

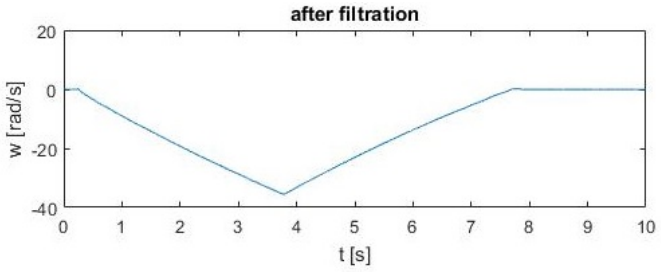

Figure VIII. Velocidad durante el ensayo de inercia

Este gráfico podría haber sido invertido, la disminución de la velocidad podría haber sido un aumento, esto solo tiene que ver con la dirección de rotación. El punto más bajo del gráfico muestra el momento de máxima velocidad, cuando la carga llega al suelo tras ser lanzada libremente. Las líneas no son completamente rectas, y por esta razón, el valor 20 fue elegido para los cálculos por ser la media de la inclinación, con el fin de comparar con la máxima precisión.

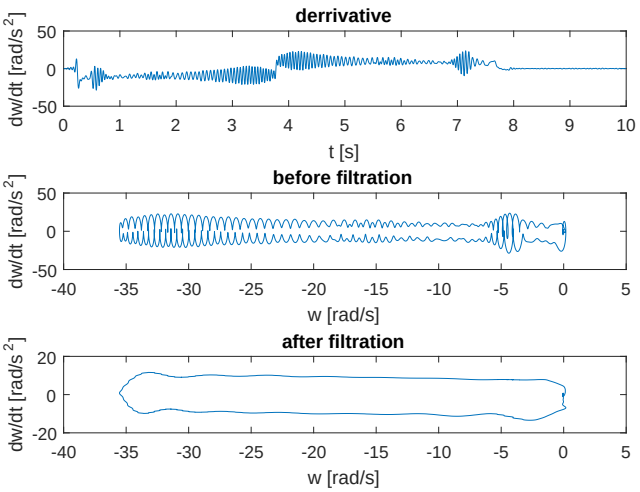

Figure IX. Aceleración de rotación durante el ensayo de inercia y Relación de la aceleración con la velocidad de rotación durante el ensayo de inercia

En estos gráficos se puede observar la relación de la velocidad de rotación con respecto a su derivada, que es la aceleración de rotación. Cuando se produce un incremento o decrecimiento de la velocidad, la aceleración es constante en valores positivos o negativos. Por medio de la conocida segunda ley de Newton se puede obtener el momento de inercia del motor estudiado $T_{dyn} = J\frac{\partial \omega_r}{\partial t}$.

D Ensayo de arranque revertido

En este ensayo el rotor está girando en una dirección y de repente es parado para empezar a girar en la otra dirección. El objetivo de este ensayo es medir el momento electromagnético.

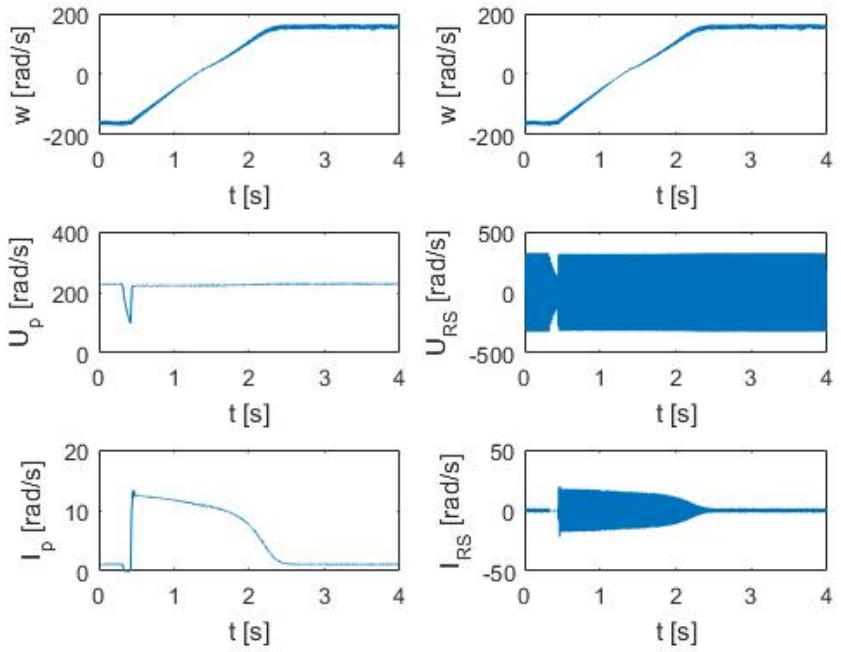

Figure X. Velocidad, voltaje y corriente durante el ensayo de arranque revertido

El cambio en la dirección de la velocidad puede apreciarse claramente por medio de los valores negativos y positivos de la gráfica de la velocidad. La corriente, al principio, se encuentra en estado estacionario y luego sufre un crecimiento debido al pseudo Start-Up y finalmente retorna a su estado estacionario. Este incremento en la corriente es incluso mayor que en un Start-Up normal ya que el deslizamiento al principio de este ensayo es mayor que uno y la corriente ha de superar esa diferencia. El cambio en el voltaje no se aprecia tan claramente debido a la existencia de cierto voltaje inducido en el núcleo.

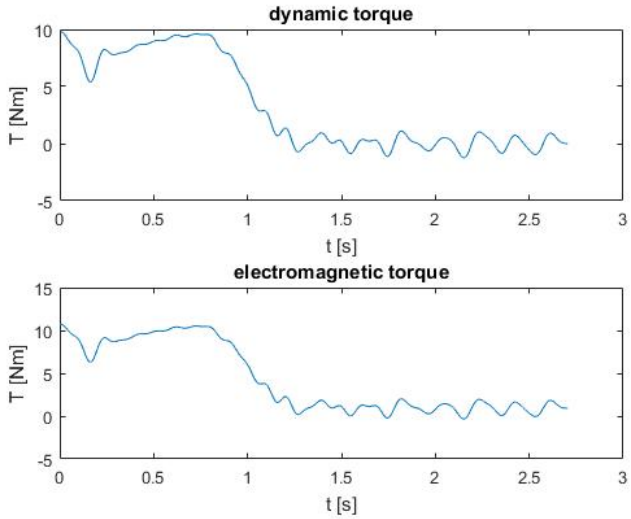

Figure XI. Comparación entre los momentos dinámico y electromagnético durante el ensayo de arranque revertido

En relación al momento dinámico, por la bien conocida segunda ecuación de Newton $T_{dyn} = J\frac{\partial \omega_r}{\partial t}$, se puede apreciar cómo las variaciones de la velocidad del rotor afectan al momento dinámico debido a su condición de derivada. En vista de los gráficos, y de la conocida ecuación $T_{em} = T_{dyn} + T_{me}$, se puede afirmar que el momento electromagnético es casi igual que el momento dinámico. El momento mecánico calculado usando la potencia mecánica hallada en el ensayo de vacío es muy pequeño en comparación con los otros dos.

V Modelo matemático del motor de inducción

La gran mayoría de las máquinas de inducción son motores trifásicos. El objetivo de esta sección es desarrollar ecuaciones para llevar a cabo varios análisis y desarrollar tareas para estos motores.

A Marco de referencia arbitrario

Las técnicas de control automático requieren modelos adecuados en los cuales las variables de interés den una respuesta constante en estado estacionario. Para controlar los motores de inducción nos encontramos con un problema debido al acoplamiento entre estátor y rotor con parámetros variables con el tiempo (inductancias) por el continuo cambio en la posición del rotor. Esto hace que las técnicas convencionales no resulten apropiadas, necesitando una transformación de ejes dentro de un marco friccional rotario arbitrario con ejes directo y de cuadratura. Estos ejes rotan a una velocidad arbitraria dependiendo de la región de operación en la que se encuentren: referencia estacionaria ($\omega = 0$) para el Start-Up, referencia síncrona ($\omega = \omega_{syn}$) para el movimiento en equilibrio, y la referencia rotor ($\omega = \omega_r$) para velocidades cambiantes por aceleración y deceleración.

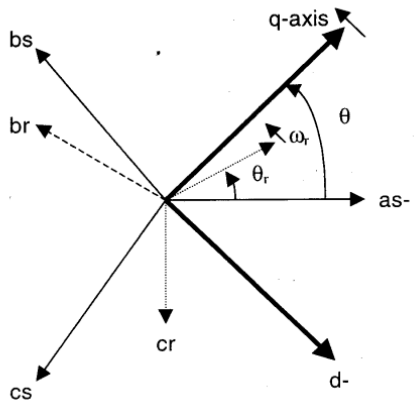

Figure XII. Marco de referencia arbitrario, qd0

No cabe duda que los voltajes reales aplicados al motor y las corrientes resultantes están en el sistema trifásico. Las cantidas qd0 se obtienen tras las transformaciones de Clarke-Park. Estos ejes cuadratura, directo y cero no pueden ser ni medidos ni obtenidos directamente. Como consecuencia, los voltajes qd0, aunque pueden ser vistos como controladores no se aplican a las fases. Este concepto de análisis fue desarrollado para reducir la complejidad matemática y hacer este análisis transitorio computacionalmente viable.

B Modelo, simulación y análisis

Como se aprecia en la figura XIII el modelo es implementado introduciendo un Asynchronous Machine Block, diseado previamente por Simulink, en el cual han sido introducidos todos los parámetros calculados en los ensayos, cuyos valores están en el marco de referencia qd0. Este bloque opera tanto en modo generador como en modo motor dependiendo del signo del momento mecánico: si este es positivo, actúa de motor, de otra

manera actuaría como generador. Los voltajes de salida de este bloque están cortocircuitados por lo que se puede ver que es un motor de jaula de ardilla, como se especifica en la sección IV.

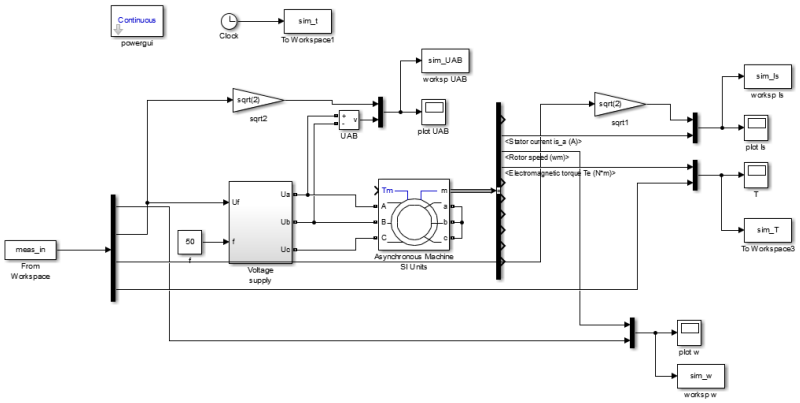

Figure XIII. Modelo matemático del motor de inducción implementado en MATLAB-SIMULINK

Otro bloque es Voltage Supply Block, con la finalidad de proveer al sistema con un voltaje de entrada igual al voltaje suministrado por la red, de otra manera, el modelo sería controlados por un voltaje sinusoidal pero sin los cambos particulares en amplitud de las mediciones reales.

En cuanto a la precisión, es bien sabido que las mediciones son más precisas que el modelo porque con tomadas directamente de la máquina. Por el contrario, el modelo no contempla muchos aspectos físicos. Algunas de las simplificaciones son las siguientes:

- Modelo monoharmónico solo basado en el armónico de 50 Hz.
- Cambios en frecuencia no considerados. Se asume una frecuencia constante de 50Hz.
- Efectos térmicos ignorados. Al aumentar la temperatura, los valores de las resistencias se incrementan.
- No todo el flujo es utilizado. Hay ciertas fugas de flujo debido a la dispersión por ranuras.
- La fricción en el eje es asumida como cero.
- Excentricidad en las máquinas no considerada. El entrehierro no tiene el mismo espesor en todas las direcciones.
- Asimetría en las fases no considerada. Esto ocurre cuando tenemos una carga no balanceada, en otras palabras, las resistencias de las fases no son iguales o los voltajes suministrados son diferentes.
- Torsión. Solo una inercia es considerada (la inercia del motor de jaula de ardilla), y sin embargo hay otra máquina, máquina DC, con otra inercia diferente conectada por medio de un eje.

VI Comparación entre el modelo y el motor real

En esta sección, dos modelos dinámicos han sido analizados. Los siguientes gráficos muestran tanto las medidas del motor real (azul) como los comportamientos de simulación (rojo).

A Start-Up state

En este estado la máquina no está en funcionamiento hasta que posteriormentese se aplica cierto voltaje consiguiendo el arranque del motor. Este estudio ha sido llevado a cabo con los valores positivos de los datos del ensayo de arranque revertido.

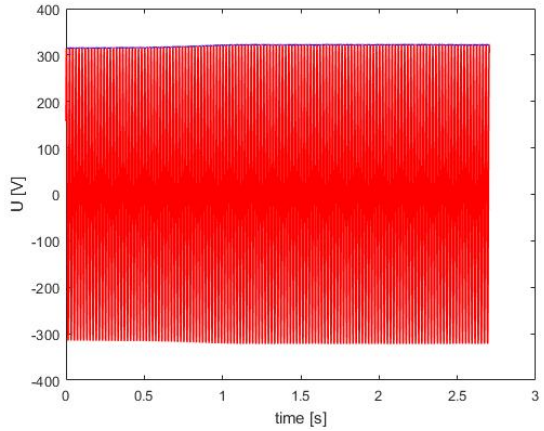

Figure XIV. Voltaje durante Start-Up

Como se puede observar, el cambio en el voltaje es instantáneo. Una vez conectada la máquina a la red, el voltaje alcanza su posición estacionaria.

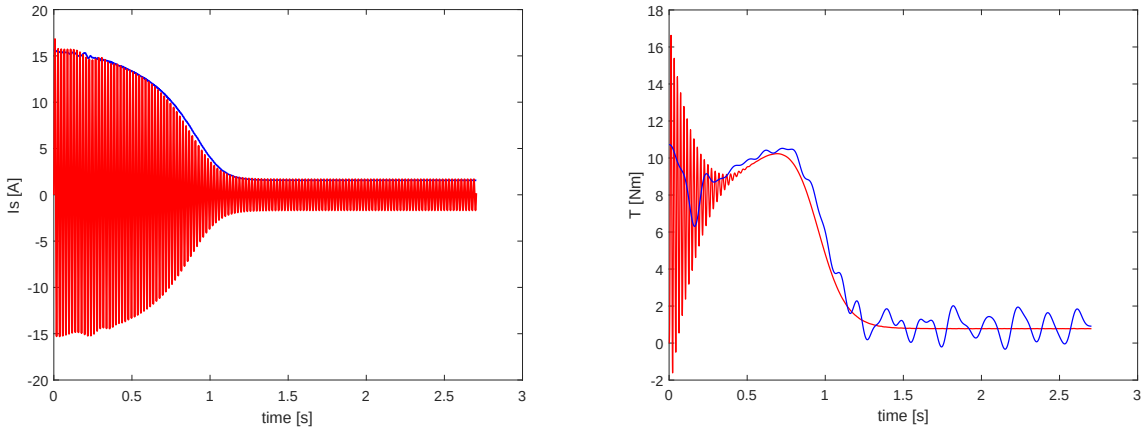

Figure XV. Corriente durante Start-Up (izquierda) y Momento electromagnético durante Start-Up (derecha)

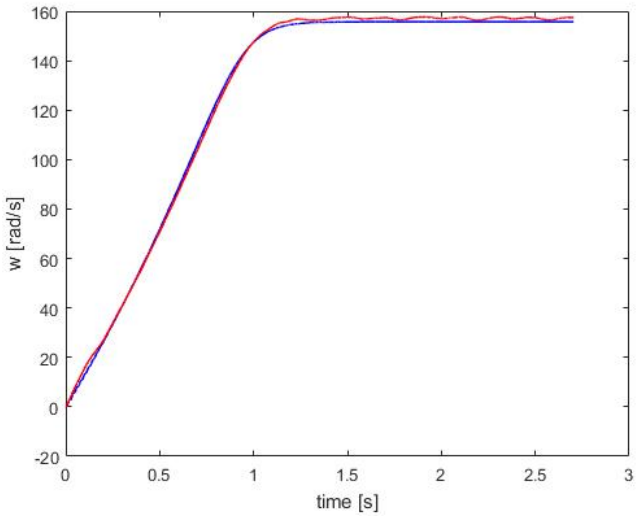

Figure XVI. Velocidad durante Start-Up

Es conocido que la corriente depende del deslizamiento, por tanto, cuando la velocidad del rotor se aproxima a la síncrona, la corriente decrece casi llegando al valor cero debido a la baja velocidad relativa, o en otras palabras, a la baja fuerza electromotriz inducida. Al mismo tiempo, se produce un decrecimiento similar en el momento electromagnético debido a la bajada de dicha corriente.

A la vista de estos gráficos, se puede apreciar que alcanzando la velocidad su estado estacionario, siendo su valor cercano al síncrono, la corriente y el momento decrecen. Esto se aprecia a partir del primer segundo.

A la luz de estos gráficos se puede afirmar que el modelo matemático elegido es altamente adecuado para este estado dinámico.

B Disconnection of three phases

En este estado de funcionamiento el motor se encuentra girando regularmente, y de forma repentina las tres fases de voltaje son desconectadas.

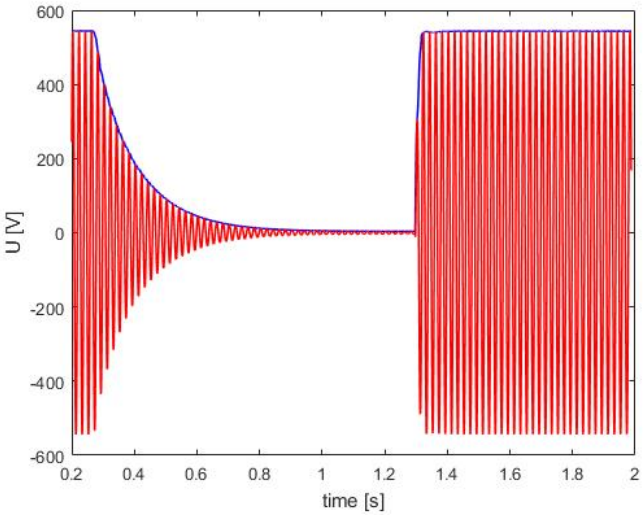

Figure XVII. Voltaje durante Disconnection of three phases

La figura XVII muestra el decrecimiento en voltaje después de la desconexión de las tres fases, lo cual puede ser apreciado después del segundo 0,25. A pesar de que la desconexión es una acción instantánea, el voltaje no decrece de la misma forma debido a la existencia de cierto voltaje remanente en el núcleo. A los 1,3 segundos, se vuelven a conectar las tres fases y el resultado es instantáneo.

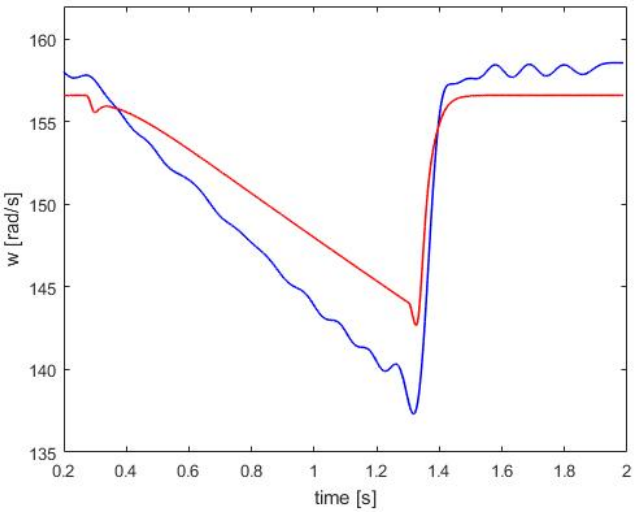

Figure XVIII. Velocidad durante Disconnection of three phases

La figura XVIII muestra la influencia que la desconexión del voltaje tiene en la velocidad del rotor. Una vez las tres fases se desconectan, la velocidad del rotor desacelera hasta su detención. Sin embargo, en este ensayo a los 1,3 segundos se conecta nuevamente el

voltaje sin dejar que el rotor se detenga. En el momento de la reconexión, el rotor gira a una velocidad de 137 rad/s aproximadamente en el motor real y a 143 rad/s en el modelo.

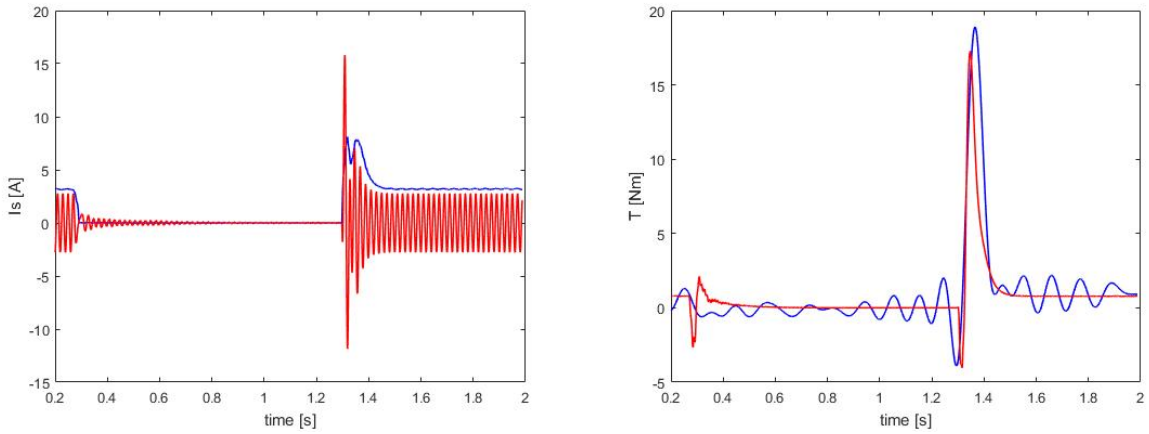

Figure XIX. Corriente durante Disconnection of three phases (izquierda) y Momento electromagnético durante Disconnection of three phases (derecha)

Como se ha explicado en la sección III, la corriente, y por tanto, el momento dependen del deslizamiento. En vista de los gráficos superiores, en el instante de desconexión, la velocidad del rotor empieza a bajar y como consecuencia se produce un decrecimiento de la corriente y del momento. Después de aproximadamente 1 segundo, el voltaje trifásico se vuelve a conectar y la corriente y el momento toman valores más altos debido al pseudo Start-Up y posteriormente retornan a sus valores estacionarios. El comportamiento de la corriente y el momento se parecen a los del Start-Up state pero con una diferencia: la velocidad del rotor no es cero en el momento de reconexión, por tanto, los valores máximos de la corriente y el momento son inferiores que en un real Start-Up.

Basándonos en los gráficos anteriores, el modelo elegido puede ser considerado moderadamente preciso. Con respecto al gráfico del voltaje; tanto en el motor como en la simulación son exactamente iguales. Por otra parte, la velocidad de rotación es ligeramente diferente por un medio u otro, alcanzando el valor más bajo (aproximadamente 137,5 rad/s) usando las mediciones del motor real y 143 rad/s por medio del modelo de simulación. Por esta razón se puede apreciar que en el motor real la velocidad decrece más rápido que en el modelo, por lo tanto, se puede constatar que el valor de inercia es mayor en el modelo. Esta diferencia puede explicarse por las simplificaciones efectuadas en el modelo. En cuanto a los gráficos de corriente y momento aunque existen pequeñas diferencias, los resultados se consideran aceptables.

VII Conclusión

Este estudio ha destacado la importancia de las máquinas de inducción, dispositivos mejorados a lo largo de los años debido a su fiabilidad y rendimiento. Por el contrario, siendo motores AC presentan problemas en el control digital. Para conseguir un modelo matemático lo más semejante a un motor real, ha de ser diseñado teniendo en consideración todas las pérdidas y la naturaleza de cada valor de entrada. El modelo matemático implementado ha sido, como puede verse en la sección V, monitorizado por el voltaje real suministrado directamente de la red, lo que hace este estudio mucho más fiable.

Atendiendo a los resultados obtenidos de las comparaciones entre el motor real y el modelo matemático en los dos estados dinámicos analizados en este trabajo: Start-Up y Disconnexion of three phases, se puede apreciar que las simplificaciones no afectan significativamente a la rigurosidad de las soluciones. A pesar de que muchos aspectos de la física no han sido considerados, los resultados son aceptables y en algunos casos altamente adecuados, lo cual puede ser observado en la sección VI. Por esta razón, los modelos matemáticos pueden ayudar a la investigación de los comportamientos de estos motores en cualquier estado dinámico y servir como una poderosa herramienta para progresar no teniendo la necesidad de llevar a cabo experimentos con el motor una vez sus parámetros hayan sido calculados por medio de los diferentes ensayos de vacío, cortocircuito, inercia y arranque revertido.

Con respecto a otros estados dinámicos, 1-phase Disconnection podría haber sido analizado. Sin embargo, estos modelos no están perfectamente adaptados para casos específicos, resultando en ocasiones, muy difícil su resolución. En conclusión, otros estados dinámicos deberían ser examinados para que el modelo pueda ser considerado un instrumento preciso sustituto de un motor real y de esta manera aprovechar las ventajas del modelo en relación a tiempo consumido, desgaste, mantenimiento, descargas eléctricas o incluso posibles averías del motor.

Identification of mathematical model parameters of induction motor

1 Introduction

Induction machines play a significant role in every application these days. Particularly, in the case of induction motors, they serve the purpose of transforming supplied electricity to mechanical energy. It is obvious that without this important scientific breakthrough, the world we live in could not be similar to what it is today. Even in fields such as speed control, in which their use has not been predominant, induction motors are now being introduced thanks to the well known variable-frequency inverters. In view of their relevance, this study was basically an experimental work set out to draw attention on their usefulness, discover the basis of their favourable outcome and establish an accurate mathematical model that can be regarded as a simplification of the reality, resulting in proper and rigorous results.

On account of the aforementioned arguments, the fundamental aim of this thesis is to shed some light on the development process of a mathematical model which resembles the real motor, despite the unavoidable physical simplifications it involves. It also encompasses the analysis and comparison of the results, explaining their causes. For that purpose, the identification of model parameters is to be performed using different types of known tests. Then, these parameters are integrated in the model as input values in order to let the investigation advance.

As far as the mathematical model is concerned, the following pages broadly explain the intrinsic simplifications due to the lack of precision in the MATLAB-SIMULINK simulations, and the transformations made to the actual input values in favour of decreasing the difficulty of the model at preparation and run-time.

With reference to the measurements, all losses have been taken into account and the majority of the signals have been filtered due to the existence of numerous signals with similar frequencies during the performance of the tests. These outer signals can affect the outcome of our investigation, therefore, the possibility of inaccuracies arising has been kept in mind during the analysis.

To summarise, this comparison could be a step further in the way induction motors have been studied for years, leading to the examination of their behaviour through simplifications, ultimately entailing an enhancement of the frequency of these investigations.

2 Induction Machines

The following section extensively covers the theoretical foundation of induction machines, emphasising their history, uses and structures.

2.1 General information

The purpose of the incoming section is to assess the current importance that induction machines have in all fields thanks to their physical specific characteristics and to give a brief overview of their history.

2.1.1 Popularity / Areas of use

The induction motor can be considered as one of the mankind's best inventions due to its simplicity and effectiveness. In addition, it is generally known that one third of the world's generated electricity is converted back into mechanical energy in induction motors. Three phase induction motors are used wherever the application depends on AC power from the national grid, being mostly used for driving machinery, pumps, fans, compressors, conveyors, elevators, hoists and also in many others routine but vital tasks.

Unlike DC motors, induction motors do not need a brush/commutator structure, which eliminates all the problems associated with sparking; such as electrical noise, brush wear, high friction, and poor reliability. The absence of magnets in the rotor and stator structures, which are susceptible to possible degradation or demagnetisation due to over temperature or over current, not only enhances reliability but makes them more economical to manufacture. For this reason, they are suitable for high power applications ranging from a few Watts to more than 10 MWatts. In high horsepower applications (such as 500 HP and higher), the AC induction motor is one of the most efficient motors, with efficiency ratings of 97% or higher, and even in most cases, efficiency can even be increased by decreasing the rotor bar resistance. Hence, they are widely used for heavy industrial applications and machinery tools.

Induction motors will continue dominating every fixed-speed application and they are also now being introduced in the speed control field, owing to the availability of reliable variable-frequency inverters. These inverters entail that induction motors can now be run from a DC source, which results in other new applications such as electric and hybrid electric vehicles.

Nevertheless, in some cases induction motors could not be well-suited to automotive applications because of the difficulties associated not only with extracting heat from the rotor, efficiency problems over wide speed and power ranges, but also due to the more expensive manufacturing process in the distribution of the windings. In contrast, permanent magnet and reluctance motors may offer better solutions for these applications. Furthermore, under light load conditions, the amount of current required to produce the rotor flux represents a large portion of the stator current, leading to a decrease in efficiency and power factor operation.

Single phase induction motors are also available. The majority of them actually have two phases, one phase is used to help the motor get started and once the motor reaches a cer-

tain speed, this phase can be disconnected leaving the motor to rotate with only one phase.

To conclude, three phase induction motors are self-starting machines. Less armature reaction and brush sparking is produced because of the absence of commutators and brushes. They are robust in construction, well-suited to higher power applications, economical and their maintenance is easier than any other electric motors.

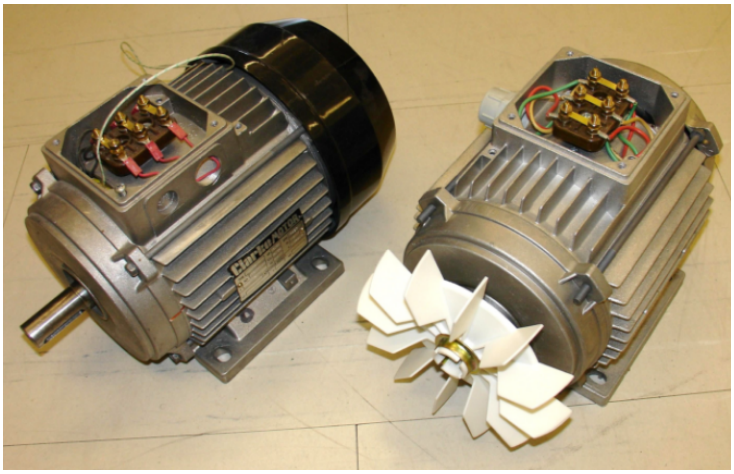

Figure 1. Induction machines, taken from [21]

2.1.2 History

The invention of the induction motor is the result of many physical discoveries and previous models. During the last few centuries there were many inventors working to discover more improvements in the electromagnetic field.

The first electric motor is known to have been designed by Andrew Gordon and Benjamin Franklin in 1740. It consisted of a type of electric motor based on the attraction and repulsion of electrical charge. Later, in 1820, Andre-Marie Ampere developed the Ampere's Law, linking together the current and the magnetic field generated around it and then, Michael Faraday, a British physic and chemist, complemented this new breakthrough explaining the conversion of electrical energy into mechanical energy. Afterwards, in 1827, Anyos Jedlik developed the very first device containing the three main components of practical direct current motors: stator, rotor and commutator, the so-called electromagnetic self-rotator. Introducing a commutator was the solution to better the problems related to repeated rotation.

An important advance in this field was made by Werner Siemens in 1856, who built an electric generator with a double-T armature winding. He is the first to place a winding into slots replacing all previous designs by this new one, which is still present nowadays in almost all electric motors. The first machines produced by Siemens, were designed to deliver pulses for telegraphs and were operated by hand, and for that reason, they did not supply continuous electrical energy. In addition to this, Siemens also developed the dynamo-electric machine, based on the double T-armature which had the downside of

producing pulsating direct current.

Another finding around 1860s is attributed to James Clark Maxwell who gathered all the knowledge of electromagnetism in four equations which are still valid today. At the same time, Znobe Thophil Gramme (Belgium) solved the same problem by the invention of the anchor ring, producing a smooth DC voltage. Nevertheless, this type of construction is no longer used. Afterwards, Riedrich von Hefner Alteneck, from 1872 to 1875, improved the double-T anchor machine, allowing the machine to produce a smooth DC voltage at the same time. Besides this, he reduced eddy currents by means of replacing solid iron core with iron wires. In the meantime, Auguste Pellerin suggested the idea of subdividing the iron core into several insulated sheets so as to avoid eddy current losses. Even so, this proposal did not get any further.

Nikola Tesla, while studying in Austria in 1882, started to think about multi-phase voltage system. After a couple of years, he emigrated to America, and in 1887 he presented his first patents for a two-phase AC system consisting of a generator, a transmission system and a multi-phase motor. He is the first to find the principles for such a transfer and to present them. Tesla 2-phase induction motor consists of a stator wounding with a pair of coils, 2-pairs of coils, one pair for each of the two phases. The individual coil is connected in series with the other coil of the pair determining both poles of the electromagnet. The two pairs of coils are oriented in the space with a difference of 90°. On Tesla's time, the source of the 2-phase voltage was a 2-phase alternator.

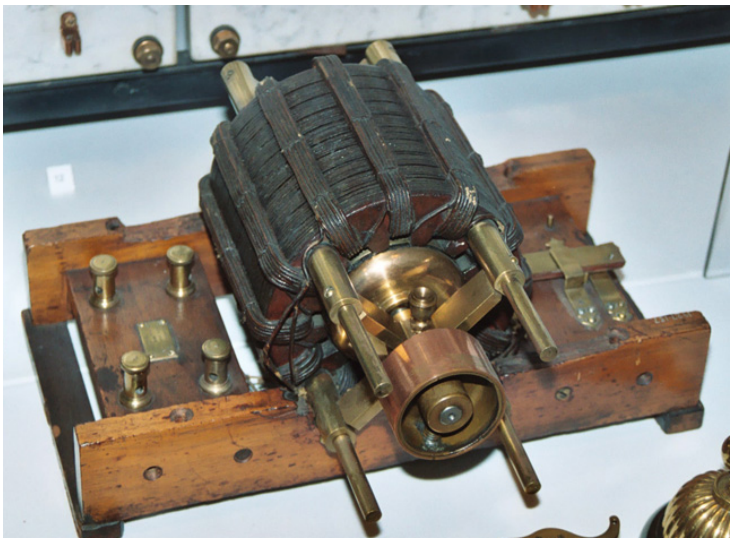

Figure 2. One of the original AC Tesla Induction Motors on display in the British Science Museum in London, taken from [22]

Beforehand, in 1885, Galileo Ferraris built the first induction motor with two phases as Tesla's one, but he thought incorrectly that induction motors could not have efficiency higher than 50%, therefore he did not attempt to improve these machines. However, by that time, Tesla did not know any of these inventions. Charles Bradley had also been investigating with multi-phase generators, he was granted several patents: firstly in two-phase and later in three-phase systems; but he did never put them into use. In 1887, Haselwander was the first to use a three-phase alternating voltage and a current system,

designing a three-phase transmission system with three-phase synchronous machines and three transmission lines, however his machine was banned for fear of disturbances on telegraph lines.

It was not until 1888 that Dolivo-Dobrowolsky improved the ideas of Tesla and Ferrari designing a three-phase cage induction motor, which is widely used nowadays. All the same, his cage induction motor did not run properly until after 1889. Not only he developed the first three-phase cage induction motor, but he also invented the three-phase slip-ring induction motor with starting resistors. For both reasons, Dolivo-Dobrowolsky must be considered as the pioneer of the three-current system.

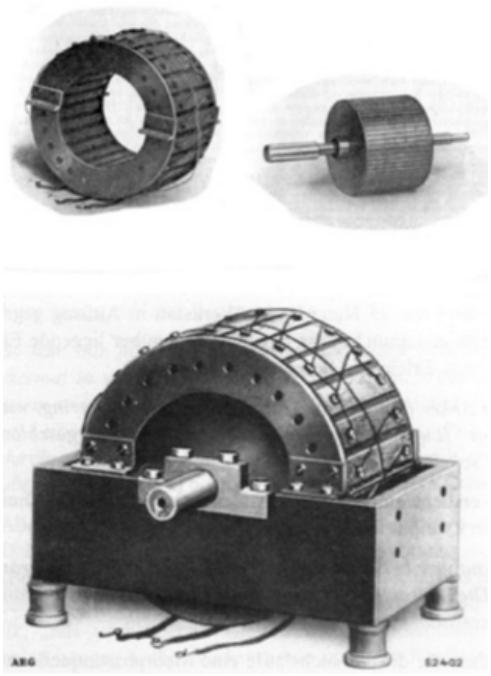

Figure 3. Dolivo-Dobrowolsky's first three-phase cage-induction motor, 1889, taken from [23]

By the year 1891, three phase induction motors went into production by General Electric, then, five years later in 1896, Westinghouse and General Electric signed an agreement for production of squirrel cage rotor.

During the last century, there have been a lot of enhancements in this field. Siemens, General Electric and other small firms were and are keeping up finding ways to create smaller and lighter motors as long as they produce power output. Some old motors from the early 1900s are still in use at historic factories and power plants.

2.2 Structure of Induction Motors (Cage and Slip Ring)

According to many books every part of an induction motor can be divided into two groups: stationary elements or rotating elements. The stationary part which is the stator and the rotating part called the rotor.

2.2.1 Stationary Part - Stator

The outer cylindrical frame of the motor is made either of welded sheet steel, cast iron or cast aluminium alloy. This may include feet, a flange or both for mounting, and has also dip-proof air intakes to improve cooling of both the stator and the rotor. This stationary part has as major constituents the stator magnetic crown and the stator winding.
The stator magnetic crown is made by stacking highly permeable laminations of steel or other ferromagnetic material(from 0,2 to 0,6 mm thick), inside the frame. Few hysteresis losses are needed as a condition when choosing a material so these laminations have to be made of soft magnetic materials due to their capacity for giving back the majority of the energy stocked during the magnetisation process. The stator magnetic crown is slotted inside letting the windings stay in, winding passes through slots of the stator.

Owing to the difference between the energy transferred to the field during magnetisation and the energy returned in the demagnetisation, some losses arise, causing overheating in the material, which is known as a form of energy dissipation. Soft magnetic materials can easily magnetise and demagnetise, they have low values of coercivity force (Hc) and high saturation; therefore, they have high magnetic permeabilities. It is observed that the value of these losses coincides with the area enclosed by the hysteresis area. These soft magnetic materials are used in cores for transformers, motors or generators due to their low overheating and their high efficiency.

The steel sheets are covered on both sides with insulating lacquer to reduce eddy current losses. Eddy currents try to oppose the cause that produces them. By means of Lenz's Law it is noted that a current passing through a conductor causes a series of flows which object to the variation of magnetic flux. These currents produce losses due to the Joule Effect. Nonetheless they have a useful application from the industrial point of view: it is in induction furnaces where, because of these eddy currents, it is possible to heat both a metal that even may get to melt. However, for electric machines, it is necessary to avoid or at least minimise the effect of these currents, which will be losses in machine performance. To do this, the following solutions are proposed:

- Core sheets: Iron cores construction consist of plates or superposed sheets with a thickness from 0,2 to 0,6 mm, isolated from one another with varnish or paper. The plates are made of a silicon steel with high resistivity, so that the intensity of the induced current decreases and so losses reach a permissible value. This construction does not produce the reduction of the magnetic flux, as it is always available along the plane that crosses the lines of force.
- Ferrite Cores: Its internal composition prevents eddy currents.
- Nuclei air: Used in very high frequencies. Since the air is an insulator, eddy currents are hardly significant.

The magnetic winding is made by joining coils to form phases. It is interesting to present the basic concepts of armature winding:

- Pole Pitch: Defined as the peripheral distance between the centre of two adjacent poles in a DC machine. It can be measured as the total number of armature slots divided by the number of poles in the machine.

- Coil span: Defined as the peripheral distance between two sides of a coil, measured in terms of the number of armature slots between them. That means, after placing one side of the coil in a particular slot, after how many conjugative slots, the other side of the same coil is placed on the armature. If the coil span is equal to the pole pitch, then the armature winding is said to be fully pitched. If the coil span is less than the pole pitch, then the winding is referred as fractionally pitched.

- Single Layer Armature Winding: Type of arrangement in which each slot is occupied by one side of an armature coil.

- Two Layer Armature Winding: Another type of layout in which every armature slot is occupied by two coil sides, one on the upper half and another on the lower half of the slot.

It will be a single-phase winding in case of single-phase motors, or a poly-phase winding in case of three-phase motors. The phases, in case of three-phase motors, can be connected in star or delta. The coils are connected to form three identical phases that have equal amplitude but different time-phase, differing by one third of a cycle. They are symmetrically displaced with respect to one another (120°), forming a balanced three-phase set. These are connected directly to a three-phase supply and each phase-winding produces an emf wave (also an air-gap flux wave) of the desired pole number. Getting the desired number of poles is not difficult, it is only about choosing the right number and pitch of the coils and by means of different arrangements of the several coils, the desired number can be reached. The stator and the rotor do not need to have the same number of phases but they are required to have equal number of poles. Disposing only one coil in one slot forming a pole, in a 4-pole winding, the first air-gap flux wave will be rectangular instead of sinusoidal, which is what it is sought. It can be enhanced by adding more coils in the adjacent slots, as long as the coils have the same number of turns in order to carry the same current. By means of this, a better wave than the original one can be obtained; but it is still to be improved. Using a two-layer a much better sinusoidal pattern can be achieved. Current in each phase pulsates at the supply frequency so the field produced by this phase pulsates in sympathy with the current in the phase.

There is no reason for the field to rotate in one phase but if the three phases are combined, a rotation comes out because the other 2 phases create the same waveform as the first phase, the only thing to take into account is that they differ in time-phase from the first current, lagging by one third and two thirds of a cycle respectively. To know the resultant field, the fields of the three phases have to be superimposed and the resultant field is not completely sinusoidal. The direction of rotation depends on which current reaches first the maximum and the following sequence. Thanks to the following chart it can be appreciated how the resultant pair of poles is formed due to the three different currents flowing through the 3-phases. Noticing at what point each current is in every specific moment, the magnetic poles formed in each phase can be easily found; therefore, the resultant magnetic pole is obtained, which is the vector of the magnetic field in this specific moment.

Access to the stator winding is provided by stator terminals located in the connexion box that covers an opening in the stator housing.

2.2.2 Rotating part - Rotor

The rotor magnetic crown is made by stacking highly permeable laminations of steel material, using the same material as in the stator. These sheets are electrically insulated from each other, coated with an oxide layer which acts as an insulator preventing undesired eddy currents, using equal or similar treatments as the ones described above. The rotor magnetic crown is slotted outside letting the electric circuit stay in. The rotor is equipped with cooling fins. At the back, there is another bearing and a cooling fan fixed to the rotor.

Depending on the constructive shape of the electric circuit of the rotor it is possible to distinguish two types of asynchronous motors:

Squirrel cage rotor (Cage motor)

This is without any doubt the most common and widely used. Its electric circuit consists of uninsulated metal bars forming the squirrel cage which resembles the rotating cages used in bygone days to exercise small rodents, this is the reason it gives that name to the rotor. These metal bars installed into the slots, commonly made of Cu or Al, are short-circuited at their two ends by conducting end-rings. In case the conductors are made of copper, the end-rings are brazed-on. Aluminium rotor bars are usually die-cast into the rotor slots, which results in a very rugged construction. Even though the aluminium rotor bars are in direct contact with the steel laminations, practically all the rotor current flows through the aluminium bars and not through the laminations. Apart from that, it is interesting to know that cage bars are arranged in an offset pattern to the axis of rotation in order to prevent torque fluctuations, this is called "skew".

This type of rotor does not have access to the induced of the rotor. It is clear due to the permanently short-circuited conductor bars that no external control can be arranged over the resistance of the rotor circuit once the rotor has been made.

Wound-rotor (Slip-ring motor)

Induced winding is a poly-phase winding, with equal or different number or phases to the stator, but with the same number of poles. This type of winding is internally connected in star and has free phase terminals connected to slip rings arranged on the shaft. Hence, the rotor circuit is open. This opening allows the increase in resistance in each phase of the rotor circuit by adding additional rotor resistance for several purposes, such as raising the torque in the start-up or decreasing the initial current. On the rubbing on slip rings, the brushes are arranged, connected to the connexion terminals arranged on the terminal board. The presence of these terminals allow us to have access to the rotor, which makes the difference between this slip-ring motor and the squirrel cage one.

The following table gathers some of the features of both types of motors.

Slip ring rotor	**Cage rotor**
Construction	
Slip rings and brushes (more complicated)	Absence of brushes and slip rings (simpler)
Rotor winding similar to stator winding	Rotor bars are short-circuited
Additional rotor resistances are possible (a high starting torque can be obtained)	Additional rotor resistances can not be added (starting torque can not be improved)
Efficiency	
Rotor copper losses are high	Less rotor copper losses (high efficiency)
Other Functional Characteristics	
Frequent maintenance (due to the brushes)	Less maintenance is required
Speed control by rotor resistance method is possible	Speed control by rotor resistance is not possible
Construction more costly	Construction cheaper
Applications	
Only used for 10% of industrial applications	Widely used
Hoists, cranes,elevators etc	Lathes, drilling machines, fans, blower printing machines etc

Table 1. Differences between Slip-ring and Cage rotors

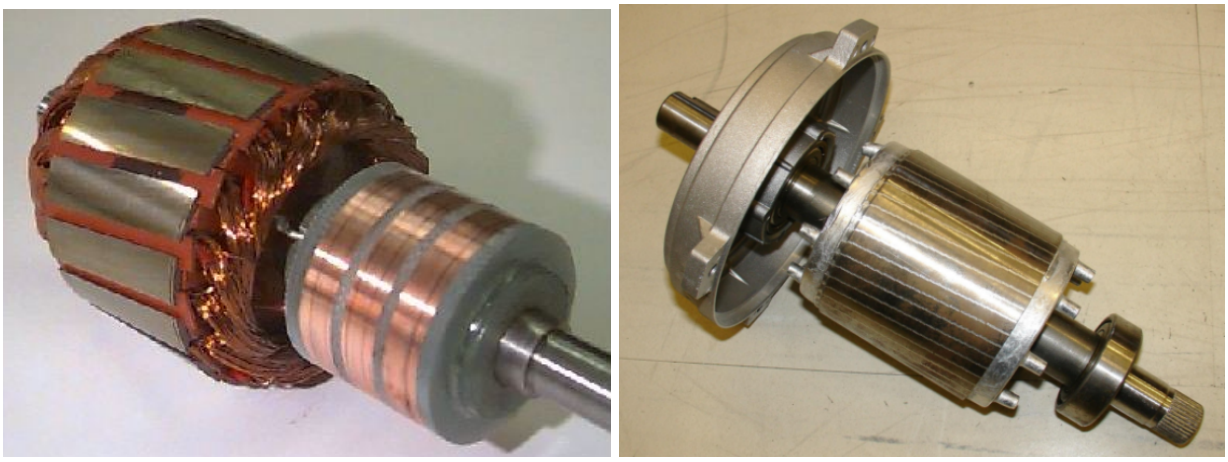

Figure 4. Slip ring rotor, taken from [32] (left) and cage rotor, taken from [25] (right)

Other parts required to complete the induction motor:

- Two end-flanges to support the two bearings.
- Bearings to support the rotating shaft in order to avoid the friction generated.
- Steel shaft for transmitting the torque to the load.
- Cooling fan to provide forced cooling for the stator and rotor. The fan is enclosed by a fan cover.
- Terminal box on top or either side to receive the external electrical connections.

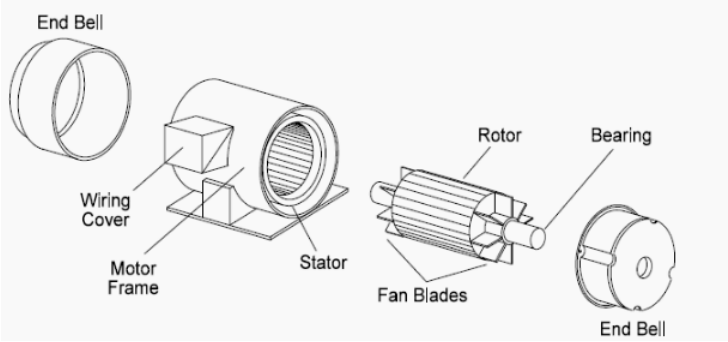

Figure 5. Other parts in induction motors, taken from [9]

2.2.3 Special Structures

In cage motors, external resistance can not be added to the rotor circuit. As the rotor has a very low resistance, the starting torque is very poor. This could be enhanced by creating a high resistance cage in the rotor but it would result in very poor efficiency during normal running conditions due to the increase in Cu losses. A step further in this investigation are special structures such as double-cage rotor and deep bars rotors. Moreover, it is possible to have a combination of both, the so-called deep bar double cage induction motor. These structures, which modify the resistive behaviour of the rotor, are intrinsic to the construction of the rotor instead of external impedances as rotor external resistances.

Double Cage Rotors

It was Mr. Boucheort who arranged two independent cages on the same rotor. The structural characteristics are explained below.

The inner cage or working cage is completely surrounded by iron, this causes the inner bars to have a much higher leakage inductance than if they were in the rotor surface. These bars are performed with a big section and high electrical conductivity materials such as Cu.

At starting:

$$s \to 0 \quad f_2 = f_1 \cdot s \tag{1}$$

Because of the slip value close to zero, the induced frequency of the emf $2\pi f = X$ in the rotor is high (equal to the frequency supplied), leading to a very high inductive impedance in the inner cage, not allowing a great current flux to pass through the bars. Most of the current passes through the outer cage with the exception of little current flowing in them. This cage concentrates the majority of the current and has the highest torque after the starting. After the starting, the closer the speed to the synchronous one, the smaller the frequency in the rotor (1). At normal running speeds, the voltage frequency of the rotor is low and both cages have negligible reactance. Thus, most of the current will flow in the inner cage due to its low resistance.

The outer cage or start-up cage is made of low conductivity materials such as bronze or brass, they produce a high resistive cage. It is designed so as to get low leakage inductance so it has a high reactance. Hence, under starting conditions, rotor current is concentrated in this cage due to its high resistivity resulting in the production of a high starting torque. Approximately, the outer cage develops a maximum torque at starting, whereas the inner cage does so at about 15% slip. This configuration provides, as it is required, the induction motor with a much higher starting torque and less starting current. It is suitable for reduced voltage starting. On the contrary, it also gives slightly worse running performance.

Deep Bar Rotors

Made by a single cage, usually of copper, deep bar rotors have deeper and narrower slots than in a conventional cage rotor.

At starting, the frequency of the rotor is the same as the frequency supplied, and the auto-inductive flux leakage in the slots leads to a current concentration in the upper area of the bars/slots. By means of this, an increase in bars resistance is generated, which results in a higher starting torque and less starting current. At normal running states, rotor voltage and current frequency is greatly low, thus, the auto-inductive effect has little importance because the current distributes itself more uniformly across the cross-section of the bars.

These rotors are well suited for those applications where there is a limitation in starting current. These motors can also be started with reduced voltage.

Deep Bar Double Cage Induction Motors

In this type of motors, bars are separated into two layers. The outer layer has bars with small cross sections and it has relatively large resistance compared to the inner one. The bars are shortened at both ends. Hence, inductance is very low. Resistance to inductive reactance ratio is high. The inner layer has large cross section bars and its resistance is very low. As flux leakage is very high, the inductance is also very high. The resistance in relation to inductive reactance is quite poor.

As far as its operational construction is concerned, at starting, the outer and the inner side bars get induced with the same frequency as the supply. However, the inductive reactance is higher in the deep or inner side bars due to skin effect of the alternating quantity, ergo, voltage and current. Therefore, the current passes through the outer side rotor bars leading to get a higher starting torque because of the high resistant materials arranged in the outer side. As the speed of rotation increases, the frequency drops to lower values and the current turns to flow through the inner side, resulting in a decrease of the torque.

3 Principles of operation of Induction Machines

Three phase Induction Motors consist of a fixed stator, a three phase winding supplied with a three phase voltage and a turning rotor. There is no electrical connexion between the stator and rotor. Rotor currents are induced through the air-gap from the stator side. This section widely addresses all the process of generation of the rotating magnetic field and exposes the different losses during the operation mode. Apart from this, characteristic electromagnetic torque is studied in the last part of this section.

3.1 Production of Rotating Magnetic Field

The stator of the motor consists of overlapping winding offset by an electrical angle of 120°. Once the primary winding or the stator is connected to a 3 phase AC source, each phase creates a waveform of the flux and the combination of the three establishes a rotating magnetic field which rotates at the synchronous speed.

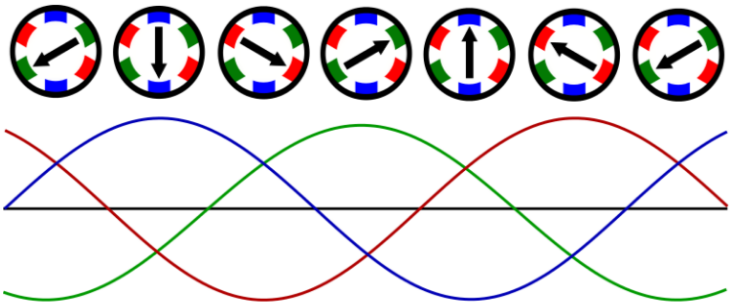

Figure 6. Production of rotating magnetic field in the stator, taken from [27]

In every electric rotating machine, the existing difference between the speed variation of electromagnetic parameters compared with the one of the mechanical parameters (angular position)must be considered. In one revolution of the rotor, conductors shift 360° mechanical degrees and at the same time, they determinate one emf cycle which corresponds to 360e of the emf waveform. Thus, in this layout the speed of variation is equal, the two parameters (electromagnetic and mechanical) rotate simultaneously. However, in case the machine had 4 poles (2 pair of poles), in each revolution, two cycles of emf would be generated (720e) modifying the electromagnetic variables at double speed in comparison with the previous case. The electrical and mechanical degrees are related to each other by the number of poles the machine has. Consequently,the frequency can be defined as:

$$f = \frac{number\ of\ cycles}{revolutions} = \frac{revolutions}{seconds} = p \cdot n \tag{2}$$

Therefore, the synchronous speed can be calculated as it is shown below:

$$N_s = \frac{60 \cdot f}{p} \tag{3}$$

According to Faraday's law, an emf induced in any circuit is due to the rate of change of magnetic flux leakage through the circuit. No matter how the change has been generated.

The change could be produced by changing the magnetic field strength, moving a magnet toward or away from the coil, moving the coil into or out of the magnetic field, rotating the coil relative to the magnet, etc.

In this type of machines, the emf is generated owing to the relative movement, cutting the field lines, of the electrical conductors immersed in the magnetic field.

$$\vec{e} = l \cdot (\vec{v} \times \vec{\beta}) \cdot \cos\theta \tag{4}$$

Being the rotor stopped $N_2 = 0$ and the field rotating at synchronous speed N_s, rotor conductors will cut the magnetic field at an speed $v\,(m/s)$, which has contrary direction to the rotation of the field, inducing in themselves an emf. This is the relative speed between the rotating flux and static rotor conductor which is the cause of current generation. Therefore, as per Lenz's Law the rotor will rotate in the same direction to reduce the cause, ergo, the relative velocity. When an emf is generated by a change in magnetic flux according to Faraday's Law, the polarity of the induced emf is such that it produces a current whose magnetic field opposes the change which produces it. This is based on the idea that induced magnetic field inside any loop of wire always acts to keep the magnetic flux in the loop constant.

On account of the fact that rotor conductors are short-circuited, a current will pass through them. This current will determine a mechanical force (Biot& Savart's Law) which will make the rotor rotate in the same direction as the field rotates. The mechanical force depends on the existence of the current and this, on the existence of the emf; hence, rotor can never reach the synchronous speed. According to Biot& Savart's Law: if current flows through an electrical conductor immersed in a magnetic field, a mechanical force is generated in the conductor.

$$\vec{F_{me}} = l \cdot (\vec{I} \times \vec{\beta}) \cdot \cos\theta \tag{5}$$

Thus from the above paragraphs, it may be noticed that the rotor speed should not reach the synchronous speed produced by the stator. If it happens, there would be neither relative speed, nor emf induced in the rotor, nor current would be flowing which would generate no torque. The difference between the stator (synchronous speed) and rotor speed is called the slip. The rotation of the magnetic field in an induction motor has the advantage that no electrical connections need to be made to the rotor in order to generate a rotation on it.

$$s = \frac{N_s - N_2}{N_s} \tag{6}$$

To summary, the stopped induction motor behaves like a transformer shorted on the secondary winding, being the stator winding like the primary winding, and the rotor like the secondary winding. As it is shorted, its internal rotor current depends on the induced voltage and its resistance. A torque is generated due to the interaction between the magnetic flux and the current conductors in the rotor. As the rotor can not reach the synchronous speed, there is always a slip which depends on the load and as the slip changes

due to changes in the load the voltage induced in the rotor winding changes leading a change in the rotor current and also in the torque. The electrical output of the stator generated by the power supply is converted through the air gap into mechanical power in the rotor. The stator current therefore consists of two components, the magnetization current and the actual load current.

3.2 Energetic Balance in Induction Motors

Electromechanical and electromagnetic transformations are accompanied by unavoidable losses which turn into heat producing increases in temperatures in different parts of the electric machine. Rotor speed in induction motors is less than the synchronous of the rotary magnetic field by the amount of slip which means that rotor power is also less than the electrical input power provided by the magnetic field. This difference in power is lost in the rotor windings as heat, thus, copper losses are proportionately dependent on the slip. From this clarification, it can be asserted that at the instant of the starting process (s = 1), all power induced in the rotor is converted into heat resulting in a great thermal danger. In reverse start tests, currents can get ever higher values than in start-up leading to a greater danger. Moreover, conventional self-ventilated motors do not provide adequate cooling when stopped.

The efficiency of an induction motor is related to the input power and the output power, or in other words, the electrical power supplied by the network and mechanical power generated in the shaft respectively. It can be calculated by the following formula

$$\eta(\%) = \frac{P_{input}}{P_{output}} = \frac{P_{electrical}}{P_{mechanical}} \tag{7}$$

Three phase induction motors present the following losses:

- Copper losses in the first-stator winding P_{Cu1}
- Copper losses in the second-rotor winding P_{Cu2}
- Iron losses in the stator P_{Fe1}
- Iron losses in the rotor P_{Fe2}
- Mechanical losses due to the friction in the rotating shaft P_{me}

At the top of the next page, the energetic balance in induction motors is shown, explaining where each loss is produced.

3.2.1 Copper losses–Joule Effect

Generated by the resistance, belongs to the conductors, against the current flux. These losses are also so-called Copper losses because copper is the most widely used material in the manufacture of these electrical windings. Al could also be used in specific cases.

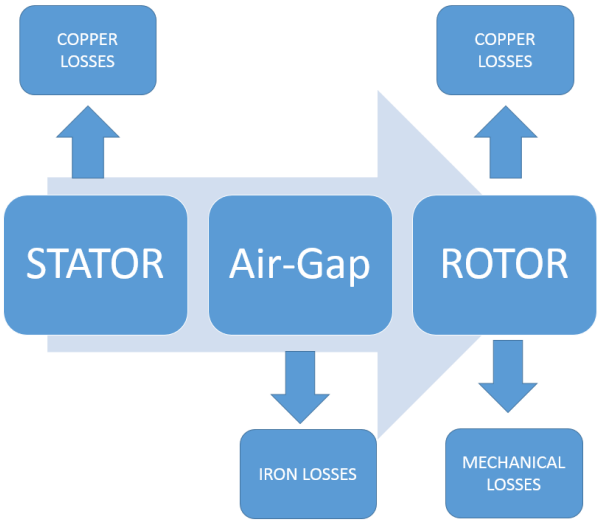

Figure 7. Energetic balance in induction motors

Joule Effect is also known as Resistive Heating, and it is produced when a current flows through a resistance producing a voltage drop and therefore, some heat is released.

This power loss can be expressed as:

$$P_{Joule} = P_{Cu} = V \cdot I = I^2 \cdot R \tag{8}$$

3.2.2 Iron losses

Generated by two magnetic phenomenons which are magnetic hysteresis and eddy currents, both depend on voltage and frequency, therefore, during operation are roughly constant. In the rotor, these losses are insignificant due to the low frequency of the rotor current.

- Magnetic hysteresis: energy loss in the magnetic hysteresis of a ferromagnetic material due to the accumulated energy during the process.

$$P_{MH} = K_{MH} \cdot f \cdot \hat{\beta}^{\alpha} \cdot W_{Fe} \tag{9}$$

- Eddy currents: energy loss in the ferromagnetic material due to flux variation which will generate an induced emf, eddy currents and finally, joule effect losses.

$$P_{EC} = K_{EC} \cdot f^2 \cdot \hat{\beta}^2 \cdot W_{Fe} \tag{10}$$

Thus, the total Iron losses are the addition of them:

$$P_{Fe} = K_{MH} \cdot f \cdot \hat{\beta}^{\alpha} \cdot W_{Fe} + K_{EC} \cdot f^2 \cdot \hat{\beta}^2 \cdot W_{Fe} \tag{11}$$

Iron losses in one state can not be higher than the value of them in nominal state, in other words, with the nominal frequency and voltage supplied. From the equations above, it is clear that iron losses can be regulated by means of modifying the frequency and voltage supplied, in order to get a lower value of them.

Being

$$U \simeq E = K \cdot \hat{\beta} \cdot f \longrightarrow \hat{\beta} = K \cdot \frac{U}{f} \tag{12}$$

With $U = U_{nom}$ and $f = f_{nom}$ it is obtained $P_{Fe} = P_{F}e_{nom}$

3.2.3 Mechanical losses

Generated by the unavoidable friction between stationary and rotating elements. Friction between the rotating parts and the air, and power loss for the self-ventilation are also taken into consideration.

Friction losses can be considered as:

$$P_{frict} = K \cdot n_{turn} \tag{13}$$

Self-ventilation losses depend exponentially on the speed, depending the exponent on the type of fan (axial,centrifugal).

$$P_{vent} = K \cdot n_{turn}^{\alpha} \tag{14}$$

The total mechanical losses can be defined as the sum of both previous losses:

$$P_{mechanical} = K \cdot n_{turn} + K \cdot n_{turn}^{\alpha} \tag{15}$$

3.3 Electromagnetic Torque

The mechanical force presented in every rotor conductor will determinate a torque. The total torque generated is the sum of the torques generated in each rotor conductor.

$$T_{em} = \sum_{i=2}^{n} (F_{mechanical_i} \times radius) \tag{16}$$

The following figure shows the typical Torque Characteristic of induction motors:

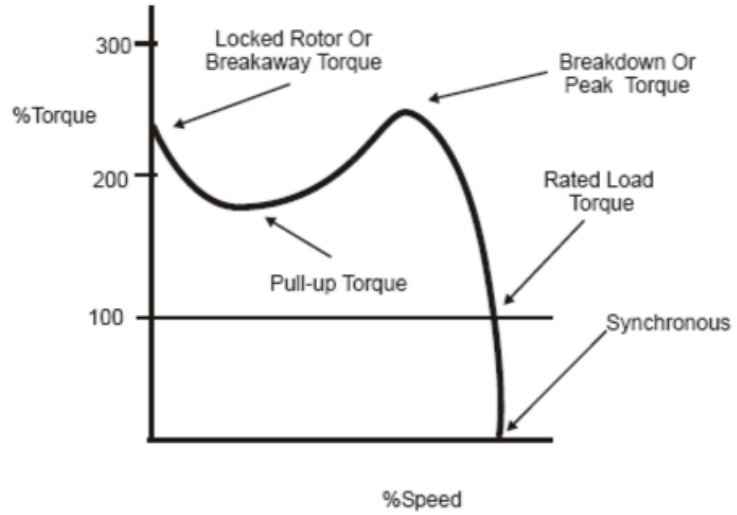

Figure 8. Torque Characteristic of induction motors, taken from [28]

Starting $s = 1$ T_B
Nominal state $s = s_{nom}$ T_N
Maximum torque s_{max} T_{max}
Synchronism $s_{syn} = 0$ T_{syn}

- Maximum or peak torque (T_{max}) is considered as the maximum value of the torque the motor is able to generate. In case the load was higher than this value, the induction motor would not be able to drive the load missing the synchronism with the net and finally, stopping.
- Starting or breakaway torque (T_B) is the torque achieved at the instant of Start-Up. Due to the slip (s = 1) it is noticeably high. During this state, the breakaway torque must be greater than the breakaway torque of the load.
- Nominal or rated torque (T_N) is achieved operating at nominal values of speed and power. A common motor has to be able to deliver the nominal torque in continuous operating without temperatures higher than the limit.
- Synchronous or no load torque (T_syn) is achieved operating at synchronous speed.
- Motor torque (T_M) must remain above the load torque during the entire acceleration phase.
- Load torque (T_L) is the counter-torque which represents the load during acceleration.
- Acceleration torque (T_a) is the difference between motor torque and load torque. It is also defined as the entire range of the torque characteristic from stop to full speed.

Operation Point

At no load the torque is very low and covers internal friction. When the motor is loaded, its speed drops slightly by the amount of slip s and the torque increases. Operation point is reached once the useful torque in the shaft is equal to the load torque resulting in the motor operating with constant speed. In case of overload the working point rises above the nominal working point but this is allowable only for a short time to avoid overheating the motor. Working point, however, should not be too low either. Below 50% of the rated load the efficiency η and the power factor $\cos\varphi$ fall dramatically and motors no longer run economically.

$$T_{useful} = T_{load} \tag{17}$$

To be clear it is necessary to employ T_{em} instead of T_{useful}.

$$T_{em}(N_2) = T_{load}(N_2) + T_{frict}(N_2) \tag{18}$$

Apart from the motor operating mode, inductions machines can operate in other two different modes depending on the slip. The figure below shows the Torque Characteristic for the different operation intervals of induction machines:

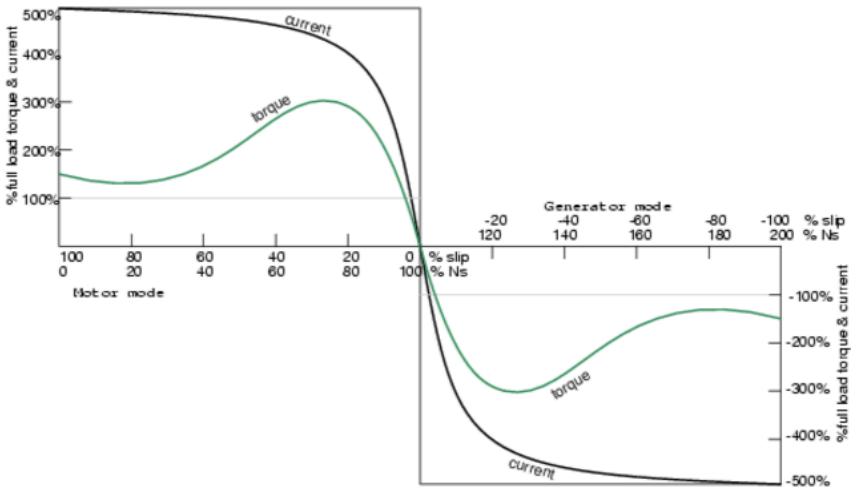

Figure 9. Torque Characteristic of induction machines in different operating modes, taken from [29]

Asynchronous or Induction Motor	$0 < N2 < N1$	$0 < s < 1$
Asynchronous Generator	$N1 < N2$	$s < 0$
Electromagnetic Brake	$N2 < 0$	$s > 1$

Table 2. Operation intervals of induction machines

4 Calculations of parameters and Results of measurements

The following section widely includes the different tests are required in order to obtain the parameters of the studied induction machine. These parameters differ from one induction machine to another, some can be dependent on temperature, permeability of the core or even on mass distribution in the machine. In terms of the tests are which are to be described below, they have to be carried out with the maximum accuracy possible. It is also suggested repeating each test, in case any mistake made either by the staff or by the machine itself.

The machine has been used for these calculations is an squirrel cage induction machine (with the stator winding connected in delta), which is arranged in connection with a DC machine. DC machine was used as a generator, producing a voltage proportional to the speed of rotation. As DC machine and induction machine share the mechanical torque and the speed of rotation; the rotor speed can be calculated by means of this layout. DC machines are not the exclusive machines which are used for this purpose, an encoder or an impulsator could have been used instead.

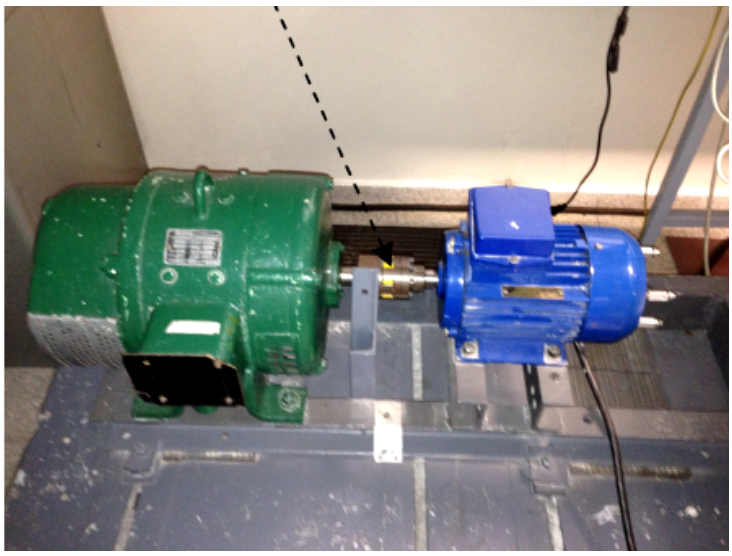

Figure 10. Squirrel cage induction motor, taken from [31]

Each machine has its nominal values, they are regarded as maximum values for which the machine is prepared. The temperature during these tests was 26 °.

Nominal values	
$P_{nom} = 1,5\ kW$	$U_{nom} = 380/220\ V$
$f_{nom} = 50\ Hz$	$I_{nom} = 6,4/3,7\ A$
$N_{nom} = 1420\ rad/s$	$\cos\varphi_{nom} = 0,8$

Table 3. Nominal values of the induction motor studied

During these subsequent tests an elliptic filter has been used in order to obtain more accurate graphs and results. Filtering is some sort of averaging the signal, here 2 times

filtering has been used so that the signal may come back to its normal state resulting in an overall phase-shift equal to zero. A low-passed frequencies filter was used with the intention of removing higher frequencies (frequencies higher than the cutting frequency which is -3 dB), hence, higher frequencies have been blocked letting only low frequencies pass.

The equivalent circuit of an induction motor can be defined as:

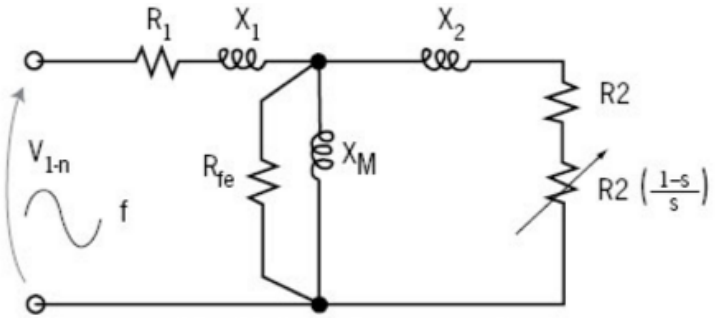

Figure 11. Equivalent circuit of induction machine, taken from [26]

Dependent on the way the motor is connected either in delta or in star, the following relations should be taken into account:

$$\begin{array}{lll} \text{Delta connexion} & \rightarrow & U_L = U_p \quad I_L = \sqrt{I_p} \\ \text{Star connexion} & \rightarrow & U_L = \sqrt{U_p} \quad I_L = I_p \end{array}$$

All devices measure line values

4.1 No Load test

No load test is carried out feeding the stator with nominal value of the voltage and removing any load from the shaft, leaving the rotor free. By means of this, the aim of this test can be achieved which is to determine the excitation impedances and the iron and mechanical nominal losses. It can be performed whether it is necessary to obtain iron and mechanical losses jointly or not. Iron and mechanical losses can be separated by performing either defective/faulty rotor test or no-load test with decreasing voltages. Measuring devices are arranged so as to get the voltage, current and power values taken during this test.

4.1.1 Defective/Faulty motor test

As in every no-load test, the stator is fed with nominal voltage and another motor is coupled to the shaft in order to make our rotor rotate at synchronous speed. Since the defective/faulty motor overcomes the friction, only iron losses are taken from the grid. Therefore $W_1 + W_2 = P_{Fe}$

Following the assumptions described above:

$$N_{2Faultymotor} = N_{2synch} \rightarrow s = 0 \rightarrow R'_c = R'_2(\frac{1}{s} - 1) = \infty \rightarrow I_{20p} = 0 \ A \tag{19}$$

$$\left.\begin{aligned} P_0 &= P_{Fe0} = 3 \cdot R_{Fe} \cdot I^2_{1Fe0p} \\ I_{1Fe0p} &= \frac{U_{10p}}{R_Fe} \end{aligned}\right\} \quad R_{Fe} = \frac{U_{10p}}{I_{1Fe0p}} = \frac{P_0}{3I^2_{1Fe0p}}$$

$$\left.\begin{aligned} P_0 &= 3 \cdot U_{10p} \cdot I_{10p} \cdot \cos(\varphi_0) \\ \varphi_0 &= \arccos \frac{P_0}{3 \cdot U_{10p} \cdot I_{10p}} \end{aligned}\right\} \quad \left.\begin{aligned} I_{1FeOp} &= I_{10p} \cos \varphi_0 \\ I_{1\mu Op} &= I_{10p} \sin \varphi_0 \end{aligned}\right\} \quad \left.\begin{aligned} R_{Fe} &= \frac{U_{10p}}{I_{1Fe0p}} \\ X_\mu &= \frac{U_{10p}}{I_{1\mu 0p}} \end{aligned}\right.$$

Constructively, low voltages drops are achieved due to the resistances and the flux leakages:

$$\begin{aligned} (R_1 + jX_1) \cdot \vec{I_{1N}} &\approx< 0.03 \cdot U_{1N} \\ (R_2 + jX_2) \cdot \vec{I_{2N}} &\approx< 0.03 \cdot U_{2N} \end{aligned} \tag{20}$$

Similarly, iron and copper losses are also low:

$$\left\{\begin{aligned} P_{CuN} &\approx< 0.02 \cdot P_N \\ P_{FeN} &\approx< 0.01 \cdot P_N \\ I_{10} &\approx< 0.1 \cdot I_N \end{aligned}\right.$$

According to the assumptions taken above; the current measured with the ammeter would be the no-load current, equally, the voltage would be no load voltage which is the nominal voltage and the power taken from the motor would actually come from the nominal iron losses.

4.1.2 No load test with decreasing voltages

The stator is fed with decreasing voltages starting from the nominal voltage or even a higher value. The lowest voltage has to be enough to keep the shaft speed the most similar to the one achieved with nominal voltage. On account of the high similarity between the different rotating speeds, mechanical losses will have nearly the same value for each speed. Thus, with the data obtained, a graphic is performed $P_0 = f(U_0)$.

$$\begin{aligned} N_{20} \rightarrow N_{2synch} \rightarrow s \rightarrow 0 \rightarrow R'_c = R'_2(\frac{1}{s} - 1) >> ... \\ ... >> (R'_2, R_1, X_1 + X'_2) \rightarrow (R'_2, R_1, X_1 + X'_2) \approx negligible \end{aligned} \tag{21}$$

$$P_{frict} = 3 \cdot U_{10p} \cdot I_{20p'} \cos[(U_{10p}, I_{20p'}) \approx 0°] = 3 \cdot U_{10p} \cdot I_{20p'} \tag{22}$$

$$I'_{20p} = \frac{P_{frict}}{3 \cdot U_{10p}} \tag{23}$$

Then, we obtain:

$$\left.\begin{array}{l} P_0 = 3 \cdot U_{10p} \cdot I_{10p} \cos\varphi_0 \\ P_0 - P_{frict} = P_{Fe0} \\ I_{1Fe0p} = I_{10p} \cos\varphi_0 - I'_{20p} \\ I_{1\mu 0p} = I_{10p} \sin\varphi_0 \end{array}\right\} \begin{array}{l} R_{Fe} = \dfrac{L_0}{3 \cdot I^2_{1Feop}} = \dfrac{U_{10p}}{I_{1Fe0p}} \\ X_\mu = \dfrac{U_{10p}}{I_{1\mu 0p}} \end{array}$$

This type of no load test was the one which has been used in order to obtain the results. The graphs below display different signals measured.

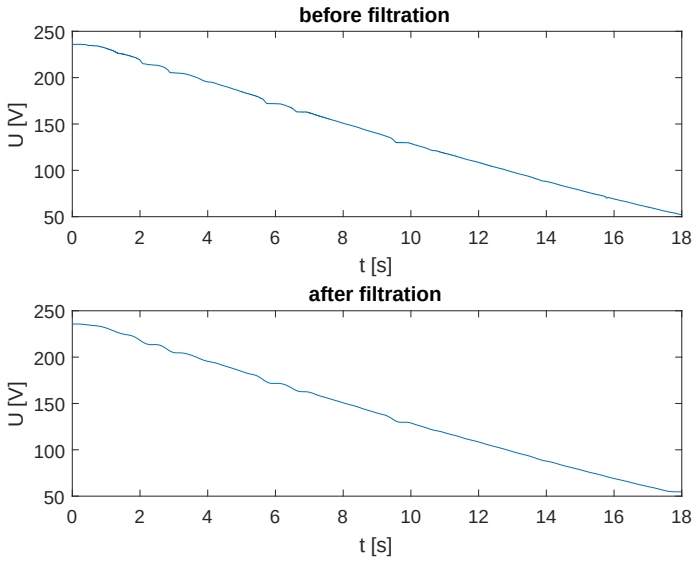

Figure 12. Time domain no load voltage signal

This graph shows the decrease in voltage made in order to accomplish this test.

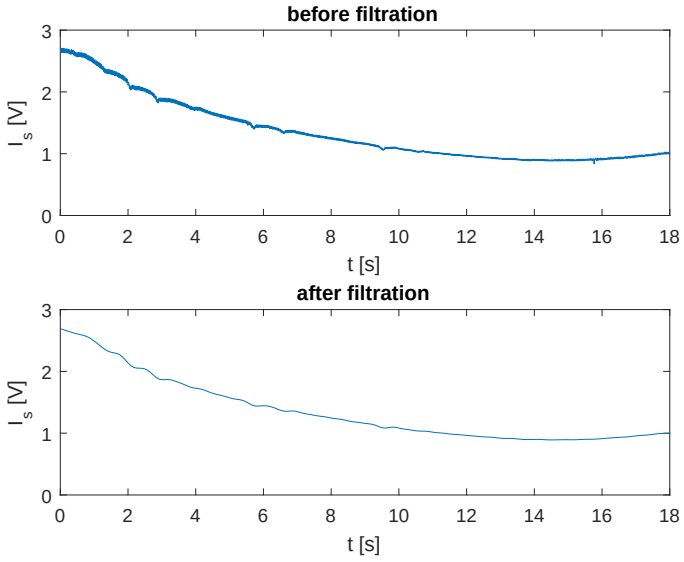

Figure 13. Time domain no load current signal

It is appreciated how the current in the stator decreases as the voltage decreases.

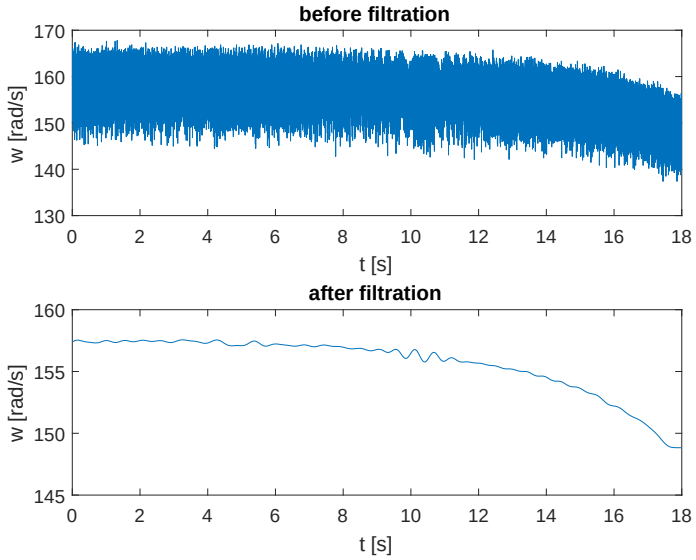

Figure 14. Time domain no load speed of rotation signal

It is obvious that when the voltage, and subsequently the current, decrease, the speed decreases. Despite this, the lessening in the voltage is quicker than the decrease in speed, this takes much more time as it can be noted.

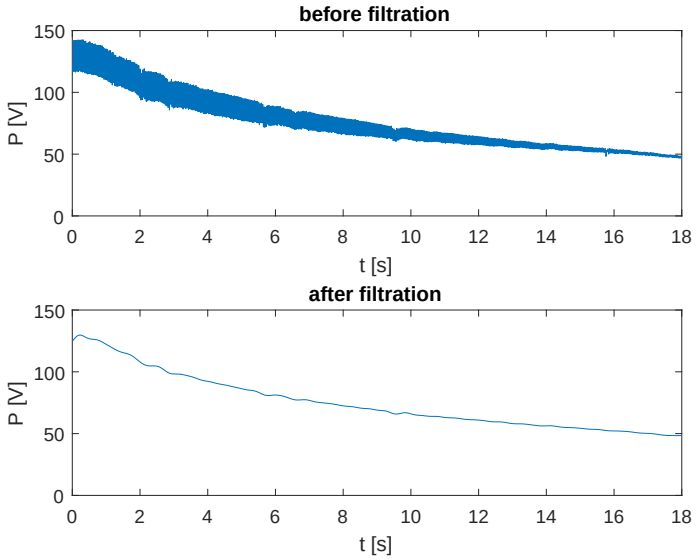

Figure 15. Time domain no load power signal

As it is well known that $P = U \cdot I$, it is clear from the above graph that the power decreases when both current and voltage values get down.

As it has been taken out the copper losses, the only losses which has to be taken into consideration are iron and mechanical losses. The following graphs display the relation between the sum of iron and mechanical losses and the square of the voltage. This relation is implemented in order to obtain an straight line by means of which separate iron and mechanical losses.

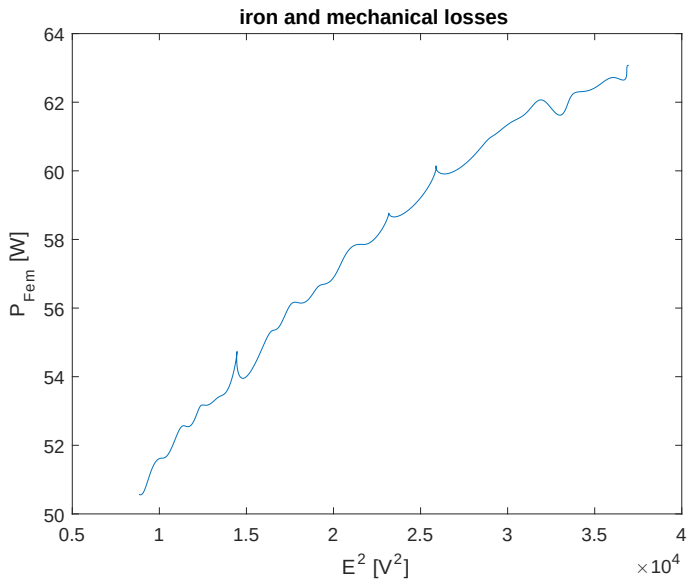

Figure 16. Iron and mechanical losses vs the square of the induced electromagnetic force during no load test before filtering

This graph shows the actual response to the measurements, before filtering. The following one comes after filtering which helps the separation.

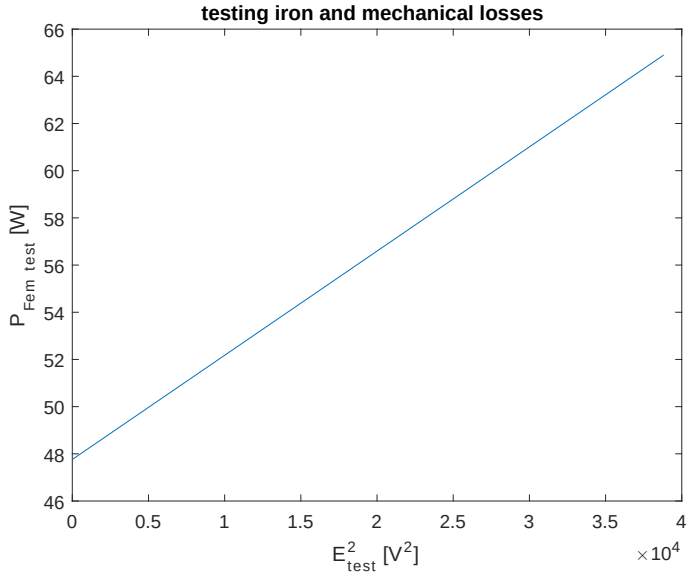

Figure 17. Iron and mechanical losses vs the square of the induced electromagnetic force during no load test after filtering

It can be assumed that the more the voltage applied, the more iron losses are going to be generated, at least before the core is saturated. Therefore, iron losses are proportional to the voltage. Regarding mechanical losses, it is also known that during this test the lowest supply voltage can even maintain speed rotating at nearly the same rate it would have if it were rotating with the nominal voltage applied. Hence, mechanical losses can be considered as constant during all this test. Consequently, it is clear that mechanical losses are the intercept of the previous graph and iron losses depend on the supply voltage.

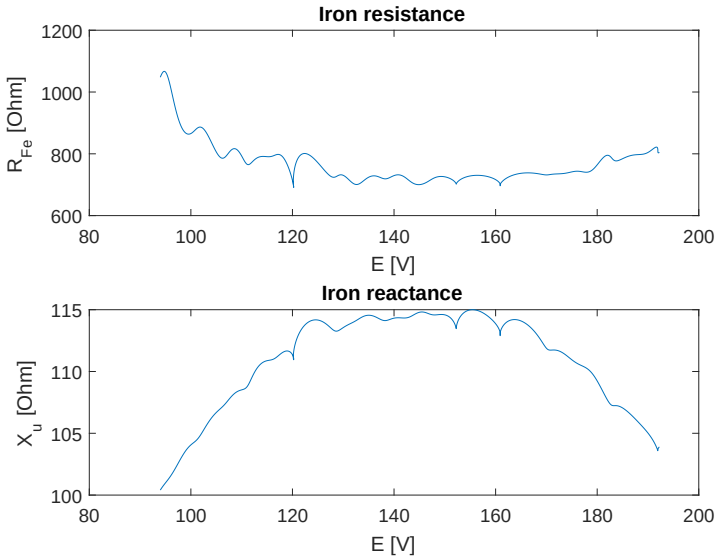

Figure 18. Relation between resistance and reactance in the iron and the induced electromagnetic force during no load test

From the lessening at the beginning in no load resistance graph, it can be seen that as voltage increases, leading to the increase in current flowing through the wires, resistance values go down so during this test as voltage is being decreases, the value of the resistance augments. However, it is also clear a little increase due to the high temperatures reached in the wires when high values of voltage are applied.

From no load reactance graph, it can be appreciated how the core is being magnetized as the voltage increases but this behaviour is not limitless. Once the core is saturated, more voltage applied does not result in a high reactance because the core can not be magnetize more. This explanation is displayed in the graph from approximately 160 V to higher values.

4.2 Short-circuit test

Short-circuit test is carried out feeding the stator with nominal value of the current and making the shaft immobilised. By means of this the goal of this test can be achieved which is to determine the winding impedances as well as the copper losses in both windings. Measuring devices are arranged so as to get the voltage, current and power values taken during this test.

$$N_{2sc} = 0 \rightarrow s = 1 \rightarrow R'_c = R'_2(\frac{1}{s_s c = 1} - 1) = 0 \tag{24}$$

$$I_{1sc} = I'_{2scp} \tag{25}$$

$$P_{sc} = 3 \cdot U_{1scp} \cdot I_{1scp} \cos\varphi_{sc} \succeq 3 \cdot R_{sc} \cdot I'^2_{2scp} \succeq 3 \cdot R_{sc} \cdot I^2_{1scp} \tag{26}$$

$$\left.\begin{aligned} \varphi_{sc} &= \arccos \frac{P_{sc}}{3 \cdot U_{1scp} \cdot I_{1scp}} \\ Z_{sc} &= \frac{U_{1scp}}{I_{1scp}} \end{aligned}\right\} \quad \begin{aligned} R_{sc} &= Z_{sc} \cos \varphi_{sc} = \frac{L_{sc}}{3 \cdot I_{1scp}^2} \\ X_{sc} &= Z_{sc} \sin \varphi_{sc} \end{aligned}$$

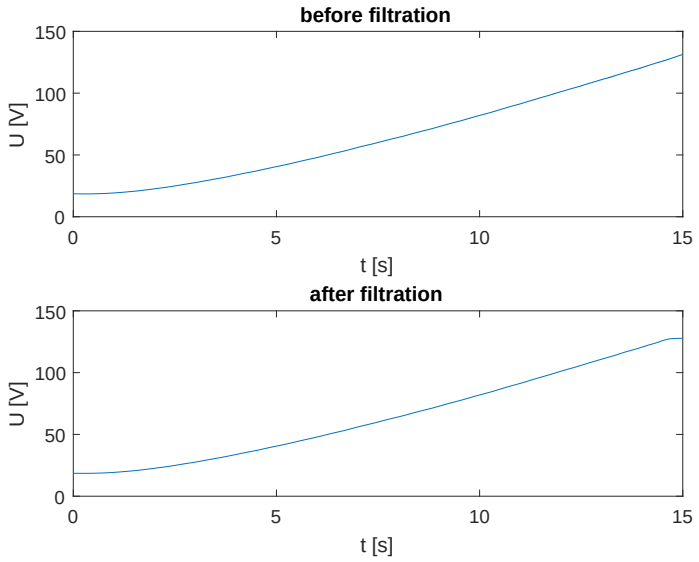

Figure 19. Time domain short-circuit voltage signal

It is shown that the voltage is increased in order to get nominal value of the current, what is needed to accomplish this test.

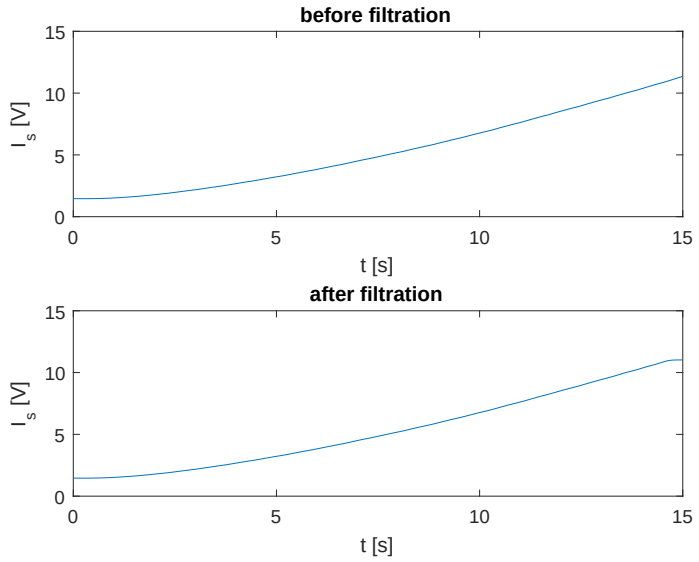

Figure 20. Time domain short-circuit current signal

During this test, the nominal value of the current has been reached which is 6,4 A and this test has been gone even further attaining higher values around 10 A. It has to be considered that a value well above the nominal could even destroy the machine.

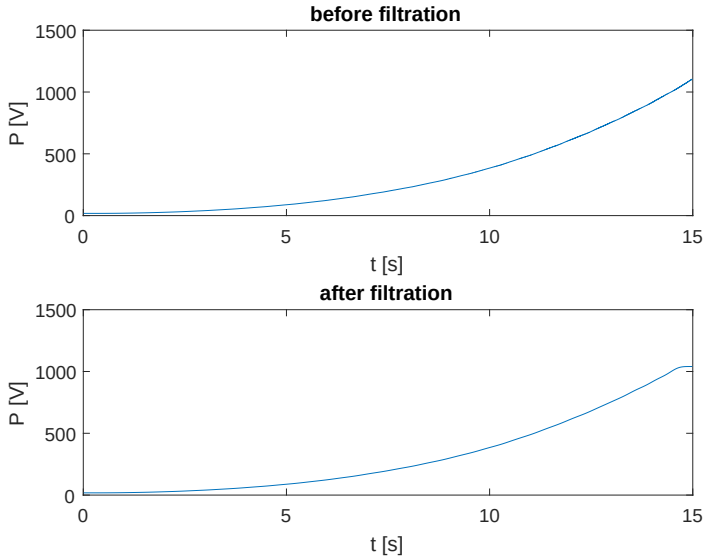

Figure 21. Time domain short-circuit power signal

Figure 21 shows the well known relation between current, voltage and power $P = U \cdot I$, as the voltage, and subsequently the current, increase in this test, the power does the same.

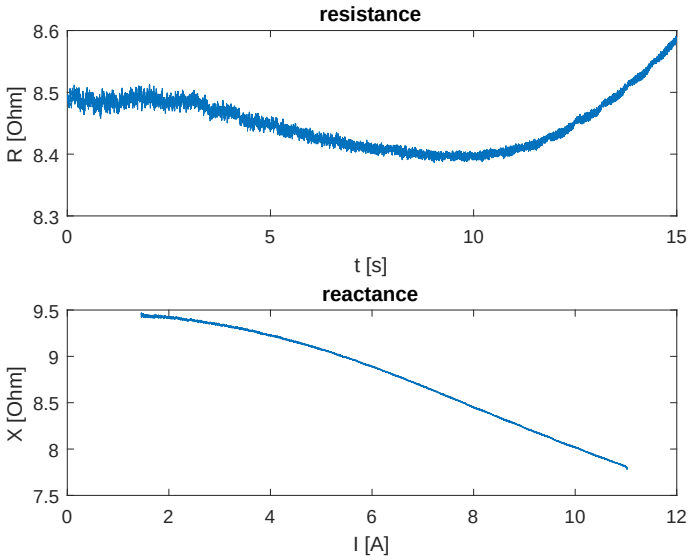

Figure 22. Time domain short-circuit resistance and reactance signals

From the short-resistance graph due to its decrease, it can be noted that voltage increases quicker than current. Despite this lessening, after 10 s approximately the resistance starts to get higher values and this tendency can be explained by the increase in temperature. It can be seen that as the temperature in the wires increases the value of resistance augments proportionately.

From short-reactance graph, it can be appreciated a decrease, but this time is more due to the permeability of the core. The permeability of the core is its intrinsic ability to support the formation of a magnetic field within itself. In other words, it is the degree of magnetisation that a material obtains in response to an applied magnetic field and it is typically represented by the Greek letter μ. As the current increases subsequently the magnetic field intensity, H, increases and finally saturation occurs. Saturation is the state reached when an increase in applied external magnetic field H cannot increase the magnetization of the material further, so the total magnetic flux density B more or less levels off. To conclude, this graph shows that the core is in saturation which means that even augmenting the current the core is not going to be magnetised more.

4.3 Inertia test

Having the machine stopped, a rope is wound around the shaft in order to raise a load from the floor to a limited height and then it is dropped freely. This test is undertaken with the aim of finding out the moment of inertia of the machine.

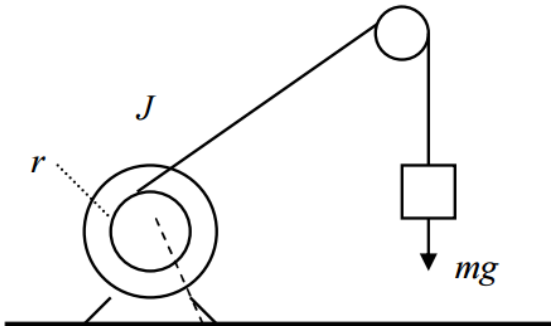

Figure 23. Inertia test, taken from [31]

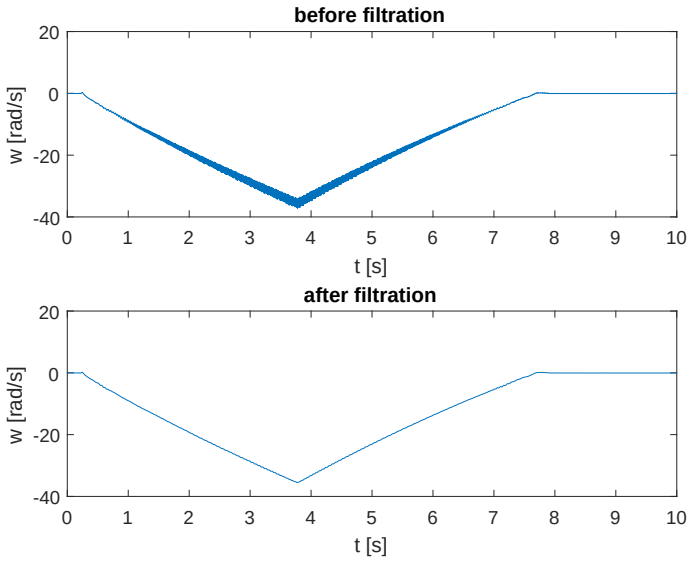

Figure 24. Time domain speed of rotation signal during inertia test

The decrease in the speed could have been an increase, it is only about the direction of the rotation. The lowest peak in the graph shows the exact moment with maximum speed when the load stops reaching the floor. As it can be observed from the graph above, the lines are not straight, hence, the slope is not completely straight. A value of 20 was chosen because it is referred to the average of inclination in order to compare with the maximum accuracy.

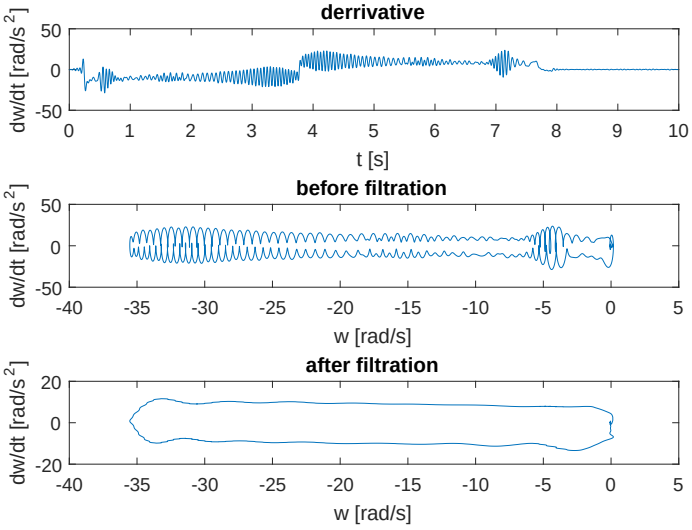

Figure 25. Time domain acceleration of rotation signal, and relation between acceleration and speed of rotation during inertia test

By the known Newton's Second Law $T_{dyn} = J\frac{\partial \omega_r}{\partial t}$, the relation between the rotor speed and its derivate which is the rotor acceleration (angular acceleration) can be appreciated. As the rotor speed decreases or increases linearly, its derivative is constant either in a positive or in a negative value. At the same time the rotor speed reaches the zero value, the acceleration also reaches it. Besides this, the rotor acceleration versus the rotor speed is also displayed.

4.4 Reverse start test

In this test the rotor is operating for a time moving in one direction and suddenly is stopped to start moving in the other direction. It is mainly carried out to measure the electromagnetic torque.

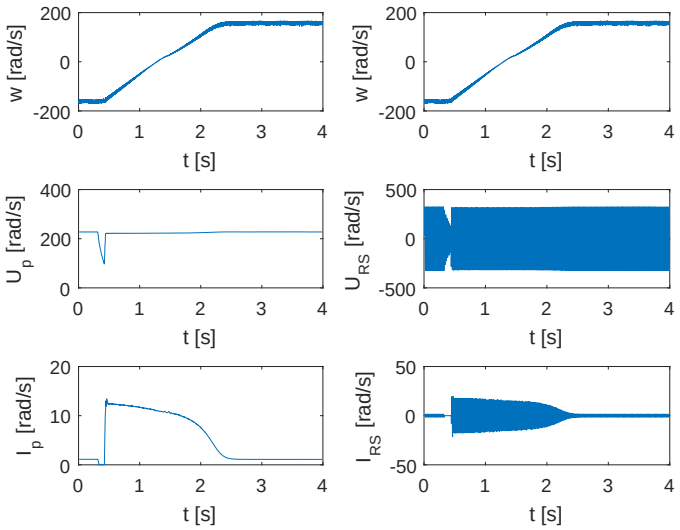

Figure 26. Time domain speed of rotation, voltage and current signals during reverse start test

The shift in the direction of the movement, by means of the negative and positive values in the speed graph, can be seen without a doubt. It is observed that at the beginning the low value of the current displays the mode of operation before the shift, after it which is produced approximately at time 0,25 s , the current increases during the start-up and finally returns to its steady state. The increase in the current during the Start-Up is even higher than in a normal Start-Up from zero because the slip during the negative values of speed is more than 1 which means that more current is needed to overcome this difference. Voltage shift is not as clear as current one due to remainder voltage induced in the core.

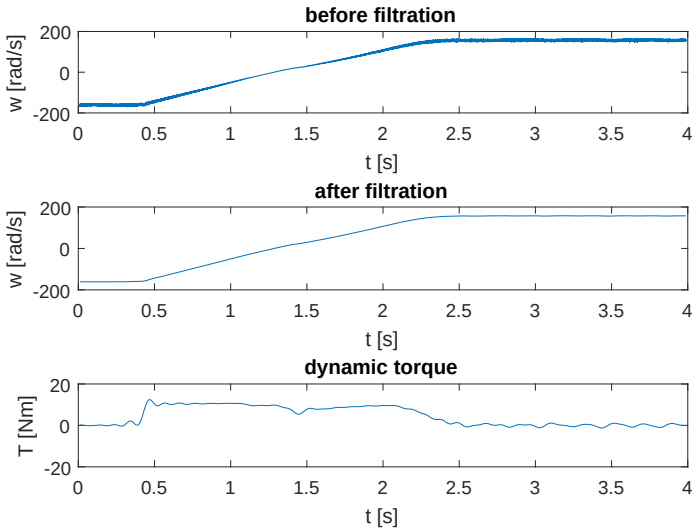

Figure 27. Time domain dynamic torque signal during reverse start test in relation to speed of rotation signal

As it is well known that $Tdyn = J\frac{\partial \omega_r}{\partial t}$, the graphics above shown that speed variations

will result in variations in the dynamic torque due to their dependency as their derivative. The time rotor speed is constant, the dynamic torque is zero. However, when rotor speed is increasing linearly during the start-up of the machine the dynamic torque is approximately constant, but not zero.

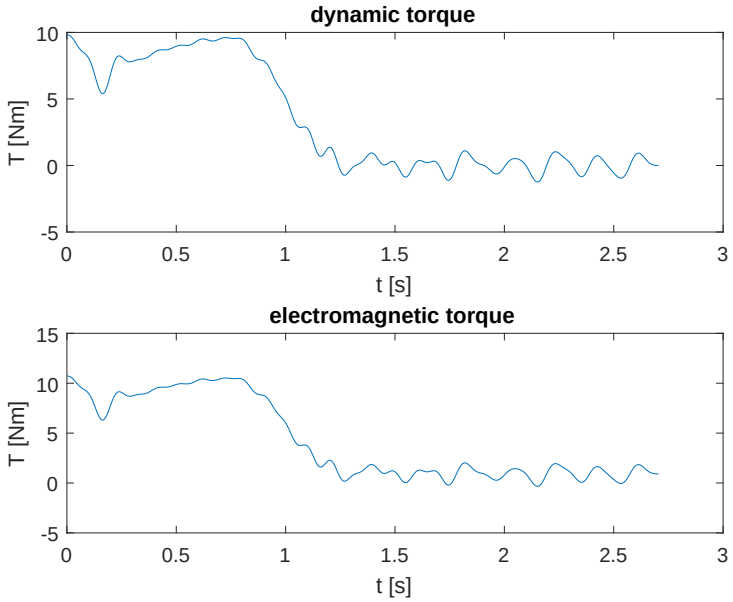

Figure 28. Comparison between dynamic and electromagnetic torque during the reverse start test

By the known equation $T_{em} = T_{dyn} + T_{me} = J\frac{\partial \omega_r}{\partial t} + \frac{P_{me}}{\omega_{Om}}$ it can be stated, in view of the graphics, that electromagnetic torque is almost equal to dynamic torque. The mechanical torque figured out using P_{me}, calculated in no load test, is low in comparison with the others.

Once, the parameters have been obtained, a simulation control can therefore be accomplished.

5 Mathematical model of Induction Motor

The vast majority of Induction machines are 3-phase induction motors. The aim of this section is to develop the equations of motion in order to carry out various analysis and design tasks for 3-phase induction motors.

The electrical DC drive systems are still used in a wide range of industrial applications even though they are less reliable than the AC drives. Their advantage consists in simple and precise command and control structures.

The AC drives, sometimes more expensive but far more reliable, require complex modern control techniques. The design of a control system is realised in two important steps:

1. The drive system has to be converted into a mathematical model, in order to accomplish the analysis and the evaluation of the system.

2. The imposed response of the drive system is obtained through an optimal regulator, when external perturbations are present.

Induction motors, especially cage motors, are relatively cheap and rugged machines because their construction is realised without slip rings or commutators. These advantages have determined an important development of the electrical drives, with induction machine as the execution element, for all related aspects: starting, braking, speed reversal, speed change, etc. The dynamic operation of the induction machine drive system play an important role on the overall performance of the system of which it is a part.

5.1 Natural Framework

Equations for the voltages supplied to the *abc* stator and rotor windings, the abc stator and rotor currents, and flux leakages are based on Kirchhoff's voltage law.

U_{as}, U_{bs}, and U_{cs} are the phase voltages supplied to the as, bs, and cs stator windings respectively, and U_{ar}, U_{br}, and U_{cr} are the phase voltages supplied to the ar, br, and cr rotor windings. As it is explained in the section 2.2, rotor bars in squirrel cage motor are short-circuited, hence, $U_{ar} = U_{br} = U_{cr} = 0$.

I_{as}, I_{bs}, and I_{cs} are the phase currents in the stator windings,and I_{ar}, I_{br}, and I_{cr} are the phase currents in the rotor windings. In the same way; ψ_{as}, ψ_{bs}, and ψ_{cs} are the stator flux leakages, and ψ_{ar}, ψ_{br}, and ψ_{cr} are the rotor flux leakages.

The *abc* stator and rotor voltages, currents, and flux leakages are used as the variables of this model.

$$U_{abcs} = r_s \cdot i_{abcs} + \frac{\partial \psi_{abcs}}{\partial t} \tag{27}$$

$$U_{abcr} = r_r \cdot i_{abcr} + \frac{\partial \psi_{abcr}}{\partial t} \tag{28}$$

Where the abc stator and rotor voltages, currents, and flux leakages vectors are:

$$U_{abcs} = \begin{bmatrix} U_{as} \\ U_{bs} \\ U_{cs} \end{bmatrix} \; U_{abcr} = \begin{bmatrix} U_{ar} \\ U_{br} \\ U_{cr} \end{bmatrix} \; I_{abcs} = \begin{bmatrix} I_{as} \\ I_{bs} \\ I_{cs} \end{bmatrix} \; I_{abcr} = \begin{bmatrix} I_{ar} \\ I_{br} \\ I_{cr} \end{bmatrix} \; \psi_{abcs} = \begin{bmatrix} \psi_{as} \\ \psi_{bs} \\ \psi_{cs} \end{bmatrix} \; \psi_{abcr} = \begin{bmatrix} \psi_{ar} \\ \psi_{br} \\ \psi_{cr} \end{bmatrix}$$

$$r_s = \begin{bmatrix} r_s & 0 & 0 \\ 0 & r_s & 0 \\ 0 & 0 & r_s \end{bmatrix} \qquad r_r = \begin{bmatrix} r_r & 0 & 0 \\ 0 & r_r & 0 \\ 0 & 0 & r_r \end{bmatrix}$$

Flux leakages can be expressed as functions of the corresponding currents in the stator and rotor using by means of the self-and mutual inductances.

$$\psi_{as} = L_{asas} \cdot i_{as} + L_{asbs} \cdot i_{bs} + L_{ascs} \cdot i_{cs} + L_{asar} \cdot i_{ar} + L_{asbr} \cdot i_{br} + L_{ascr} \cdot i_{cr} \tag{29}$$

$$\psi_{bs} = L_{bsas} \cdot i_{as} + L_{bsbs} \cdot i_{bs} + L_{bscs} \cdot i_{cs} + L_{bsar} \cdot i_{ar} + L_{bsbr} \cdot i_{br} + L_{bscr} \cdot i_{cr} \tag{30}$$

$$\psi_{cs} = L_{csas} \cdot i_{as} + L_{csbs} \cdot i_{bs} + L_{cscs} \cdot i_{cs} + L_{csar} \cdot i_{ar} + L_{csbr} \cdot i_{br} + L_{cscr} \cdot i_{cr} \tag{31}$$

$$\psi_{ar} = L_{aras} \cdot i_{as} + L_{arbs} \cdot i_{bs} + L_{arcs} \cdot i_{cs} + L_{arar} \cdot i_{ar} + L_{arbr} \cdot i_{br} + L_{arcr} \cdot i_{cr} \tag{32}$$

$$\psi_{br} = L_{bras} \cdot i_{as} + L_{brbs} \cdot i_{bs} + L_{brcs} \cdot i_{cs} + L_{brar} \cdot i_{ar} + L_{brbr} \cdot i_{br} + L_{brcr} \cdot i_{cr} \tag{33}$$

$$\psi_{cr} = L_{cras} \cdot i_{as} + L_{crbs} \cdot i_{bs} + L_{crcs} \cdot i_{cs} + L_{crar} \cdot i_{ar} + L_{crbr} \cdot i_{br} + L_{crcr} \cdot i_{cr} \tag{34}$$

$L_{asas}, L_{bsbs}, L_{cscs}$ are the stator self-inductances, whereas $L_{arar}, L_{brbr}, L_{crcr}$ are the rotor ones. On the other hand L_{asbs}, L_{ascs}, L_{bscs}, L_{asar}, L_{asbr}, L_{ascr}, L_{bsar}, L_{bsbr}, L_{bscr}, L_{csar}, L_{csbr}, L_{cscr}, L_{arbr}, L_{arcr}, L_{brcr} are the mutual inductances between stator-stator, stator-rotor and rotor-rotor windings.

Stator and rotor abc windings are identical and displaced magnetically by $2\pi/3$. Therefore, a coupling between these windings exists and their mutual inductance can be defined as:

$$L_{asbs} = L_{ascs} = L_{bscs} = L_{ms} \cdot \cos\frac{2\pi}{3} = -\frac{1}{2} \cdot L_{ms} \tag{35}$$

Being $L_{ms} = \dfrac{N_s^2}{R_m}$

$$L_{arbr} = L_{arcr} = L_{brcr} = L_{mr} \cdot \cos\frac{2\pi}{3} = -\frac{1}{2} \cdot L_{mr} \tag{36}$$

Being $L_{mr} = \dfrac{N_r^2}{N_s^2} \cdot L_{ms}$

On account of these aforementioned equations, it can be stated that self-inductance is the sum of the following two components $L_{ss} = L_{lm} + L_{ms}$. This is also applicable to the self-inductance of the rotor L_{mr}.

L_s and L_r matrix can therefore be defined as:

$$L_s = \begin{bmatrix} L_{ls} + L_{ms} & -\frac{1}{2} \cdot L_{ms} & -\frac{1}{2} \cdot L_{ms} \\ -\frac{1}{2} \cdot L_{ms} & L_{ls} + L_{ms} & -\frac{1}{2} \cdot L_{ms} \\ -\frac{1}{2} \cdot L_{ms} & -\frac{1}{2} \cdot L_{ms} & L_{ls} + L_{ms} \end{bmatrix} \quad L_r = \begin{bmatrix} L_{lr} + L_{mr} & -\frac{1}{2} \cdot L_{mr} & -\frac{1}{2} \cdot L_{mr} \\ -\frac{1}{2} \cdot L_{mr} & L_{lr} + L_{mr} & -\frac{1}{2} \cdot L_{mr} \\ -\frac{1}{2} \cdot L_{mr} & -\frac{1}{2} \cdot L_{mr} & L_{lr} + L_{mr} \end{bmatrix}$$

One obtains:

$$\begin{bmatrix} \psi_{abcs} \\ \psi_{abcr} \end{bmatrix} = \begin{bmatrix} L_s & L_{sr}(\theta_r) \\ L_{sr}^T(\theta_r) & L_s \end{bmatrix} = \begin{bmatrix} i_{abcs} \\ i_{abcr} \end{bmatrix}$$

Mutual inductances stator-rotor are periodic functions of the electrical angular displacement θ_r. They can be assumed as sinusoidal functions with 2π as the period.

$$L_{asar} = L_{aras} = L_{sr} \cos\theta_r \quad L_{asbr} = L_{arbs} = L_{sr} \cos\theta_r + \frac{2}{3}\pi \quad L_{ascr} = L_{cras} = L_{sr} \cos\theta_r + \frac{2}{3}\pi \quad (37)$$

$$L_{bsbr} = L_{brbs} = L_{sr} \cos\theta_r \quad L_{bsar} = L_{bras} = L_{sr} \cos\theta_r + \frac{2}{3}\pi \quad L_{bscr} = L_{crbs} = L_{sr} \cos\theta_r + \frac{2}{3}\pi \quad (38)$$

$$L_{cscr} = L_{crcs} = L_{sr} \cos\theta_r \quad L_{csar} = L_{cras} = L_{sr} \cos\theta_r + \frac{2}{3}\pi \quad L_{csbr} = L_{brcs} = L_{sr} \cos\theta_r + \frac{2}{3}\pi \quad (39)$$

Thus:

$$L_{sr} = \frac{N_s N_r}{R_m} = \begin{bmatrix} \cos\theta_r & \cos(\theta_r \frac{1}{2}) & \cos(\theta_r \frac{1}{2}) \\ \cos(\theta_r \frac{1}{2}) & \cos\theta_r & \cos(\theta_r \frac{1}{2}) \\ \cos(\theta_r \frac{1}{2}) & \cos(\theta_r \frac{1}{2}) & \cos\theta_r \end{bmatrix}$$

Based on the relations shown below, the electromagnetic equations can be obtained:

$$\begin{bmatrix} \psi_{abcs} \\ \psi_{abcr} \end{bmatrix} = \begin{bmatrix} L_s & L_{sr} \cos\theta_r \\ L_{sr}^T \theta_r & L_s \end{bmatrix} = \begin{bmatrix} i_{abcs} \\ i_{abcr} \end{bmatrix}$$

$$\psi_{abcs} = L_s \cdot i_{abcs} + L_s(\theta_r) \quad (40)$$

$$\psi_{abcr} = L_s^T(\theta_r) \cdot i_{abcs} + L_s \cdot i_{abcr} \quad (41)$$

Then, using the number of turns:

$$u'_{abcr} = \frac{N_s}{N_r} \cdot u_{abcr} \qquad i'_{abcr} = \frac{N_r}{N_s} \cdot i_{abcr} \qquad \psi'_{abcr} = \frac{N_s}{N_r} \cdot \psi_{abcr} \quad (42)$$

The inductances are:

$$L_{ms} = \frac{N_s}{N_r} \cdot L_{sr} \qquad L_{sr} = \frac{N_s N_r}{R_m} \cdot L_{sr} \quad (43)$$

Then:

$$L_{ms} = \frac{N_s^2}{R_m} \tag{44}$$

And as a result:

$$L'_{sr}(\theta_r) = \frac{N_s}{N_r} L_{sr}\theta_r \qquad L'_r = \frac{{N_s}^2}{N_r} L_r \qquad L'_{lr} = \frac{{N_s}^2}{N_r} L_{Ir} \tag{45}$$

$$\begin{bmatrix} \phi_{abcs} \\ \phi'_{abcr} \end{bmatrix} = \begin{bmatrix} L_s & L'_{sr}(\theta_r) \\ L'^T_{sr}(\theta_r) & L'_r \end{bmatrix} = \begin{bmatrix} i_{abcs} \\ i'_{abcr} \end{bmatrix}$$

$$\begin{bmatrix} \phi_{as} \\ \phi_{bs} \\ \phi_{cs} \\ \phi'_{ar} \\ \phi'_{br} \\ \phi_{cr} \end{bmatrix} = \begin{bmatrix} L_{ls}+L_{ms} & -\frac{1}{2}L_{ms} & -\frac{1}{2}L_{ms} & L_{ms}\cos\theta_r & L_{ms}\cos(\theta_r+\frac{2}{3}\pi) & L_{ms}\cos(\theta_r-\frac{2}{3}\pi) \\ -\frac{1}{2}L_{ms} & L_{ls}+L_{ms} & -\frac{1}{2}L_{ms} & L_{ms}\cos(\theta_r-\frac{2}{3}\pi) & L_{ms}\cos\theta_r & L_{ms}\cos(\theta_r+\frac{2}{3}\pi) \\ -\frac{1}{2}L_{ms} & -\frac{1}{2}L_{ms} & L_{ls}+L_{ms} & L_{ms}\cos(\theta_r+\frac{2}{3}\pi) & L_{ms}\cos(\theta_r-\frac{2}{3}\pi) & L_{ms}\cos\theta_r \\ L_{ms}\cos\theta_r & L_{ms}\cos\theta_r & -23\pi) & L_{ms}\cos\theta_r+23\pi) & L'_{lr}+L_{ms} & -\frac{1}{2}L_{ms} \\ L_{ms}\cos(\theta_r+23\pi) & L'_{lr}+L_{ms} & L_{ms}\cos(\theta_r-23\pi) & -\frac{1}{2}L_{ms} & L'_{lr}+L_{ms} & -\frac{1}{2}L_{ms} \\ L_{ms}\cos(\theta_r-\frac{2}{3}\pi) & L_{ms}\cos(\theta_r+\frac{2}{3}\pi) & L_{ms}\cos\theta_r & -\frac{1}{2}L_{ms} & -\frac{1}{2}L_{ms} & L'_{lr}+L_{ms} \end{bmatrix} \begin{bmatrix} i_{as} \\ i_{bs} \\ i_{cs} \\ i'_{ar} \\ i'_{br} \\ i_{cr} \end{bmatrix}$$

Finally, these relation can be obtained:

$$u_{abcs} = r_s i_{abcs} + \frac{\partial \phi_{abcs}}{\partial t} = r_s i_{abcs} + L_s \frac{\partial i_{abcs}}{\partial t} + \frac{\partial (L'_{sr}\theta_r i'_{abcr})}{\partial t} \tag{46}$$

$$u'_{abcr} = r'_r i'_{abcr} + \frac{\partial \phi'_{abcr}}{\partial t} = r'_r i'_{abcr} + L'_r \frac{\partial i'_{abcr}}{\partial t} + \frac{\partial (L'^T_{sr}\theta_r i'_{abcr})}{\partial t} \tag{47}$$

being $r'_r = \left(\frac{N_s}{N_r}\right)^2 r_r$

5.2 Arbitrary Reference Frame and Vector Control (qd0)

Traditionally, induction motors have been run at a single speed, which was determined by the frequency of the main voltage and the number of poles in the motor. Controlling the speed of an induction motor is rather more difficult than controlling the speed of a DC motor since the non-existence of linear relationship between the motor current and the resulting torque as there is for a DC motor. The technique called vector control can be used to vary the speed of an induction motor over a wide range. In the vector control scheme, a complex current is synthesised from two quadrature components, one of which is responsible for the flux level in the motor, and another which controls the torque production in the motor. Essentially, the control problem is reformulated to resemble the control of a DC motor. Vector control offers a number of benefits including speed control over a wide range, precise speed regulation, fast dynamic response, and operation above base speed.

The vector control algorithm is based on two fundamental ideas:

The first is the flux and torque producing currents. An induction motor can be modelled most simply (and controlled most simply) using two quadrature currents rather than the three phase currents actually applied to the motor. These currents are called direct I_d and quadrature I_q which are responsible for producing flux and torque respectively in the motor.

The second fundamental idea is the choice of the reference frame. The idea of a reference frame is to transform a quantity that is sinusoidal in one reference frame, to a constant value in a reference frame, which is rotating at the same frequency. Once a sinusoidal quantity is transformed to a constant value by careful choice of reference frame, it becomes possible to control that quantity with traditional proportional integral (PI) controllers.

Automatic control techniques require an accurate mathematical model so that the variables of interest may give a constant response at stationary state. To control an induction motor, an obstacle appears due to the coupling between stator and rotor with time variable parameters (inductances) because of the continuous change in rotor position. This makes conventional techniques quite difficult. For this reason, it is needed a transformation of axes within a fictional rotating frame with direct (d) and quadrature(q) axes. This arbitrary speed ω (rad/s) could be 0, ω_{syn}, ω_r depending on the region of operation: stationary reference ($\omega = 0$) for start-up, synchronous reference ($\omega = \omega_{syn}$)for equilibrium motion, and , rotor reference ($\omega = \omega_r$) for changing speeds by acceleration or deceleration.

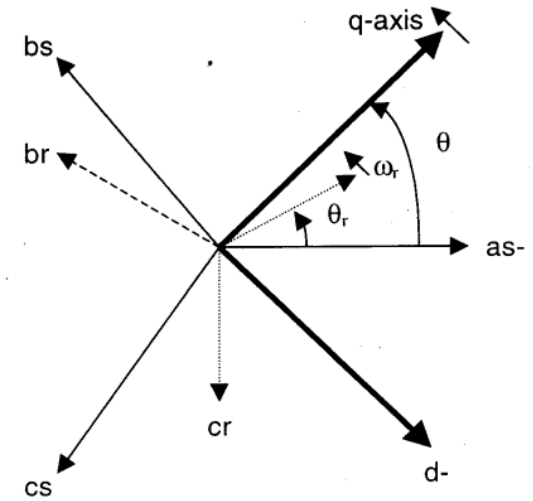

Figure 29. Arbitrary reference frame, qd0, taken from [17]

With reference to the definition, the I_q current is in phase with the stator flux, and I_d is at right angles. Needless to say that the actual voltages applied to the motor and the resulting currents are in the familiar three-phase currents. We obtain qd0 quantities which mathematically correspond to the physical machine variables as the Clarke-Park transformations are applied .

In AC machines, voltages, currents, and flux leakages are AC machine quantities. These AC phase voltages U_{as}, U_{bs}, and U_{cs} are to be supplied to the stator windings.
The quadrature, direct and zero-axis components can not be directly measured or obtained. One can not supply U_{qs},U_{ds}, and U_{eo} to the phase windings. To rotate induction motors, the AC phase voltages are supplied to the phase windings.
Therefore, the qd0 voltages, thought can be viewed as controls, are not applied to the phase windings.

This analysis concept was developed to reduce the mathematical complexity and make the transient analysis to be computationally tractable allowing analytic solutions of the resulting differential equations. Induction and synchronous machines can be examined in the arbitrary reference frame. In particular, the stationary, rotor, and synchronous frames are commonly specified.

5.3 Modelling, analysis and simulation

This section extensively addresses the layout of the implemented mathematical model, and the simplifications made through this approach. The implemented model used in this investigation is the following:

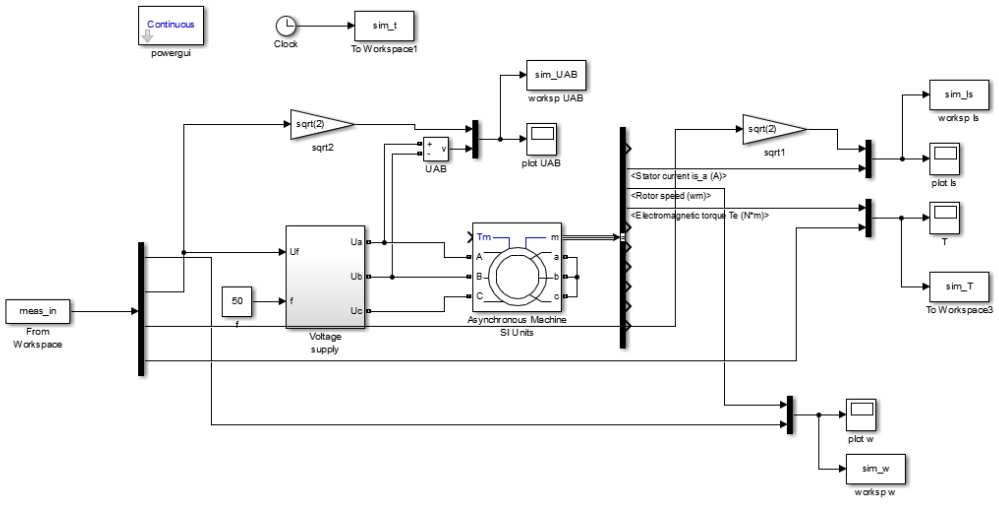

Figure 30. Mathematical model of induction motor made in MATLAB-SIMULINK

As it can be appreciated from the figure above, the model is implemented by introducing an Asynchronous Machine block already designed in Simulink in which all parameters, calculated through the different tests, have been included (this is explained in section 4). These parameters are Nominal power, voltage (line-line), frequency, Stator and Rotor resistance and inductance, mutual inductance, pair of poles, moment of inertia and factor

of friction. The last value is not being changed from the value there was before the implementation of the model. Besides these, the sample time, the rotor type, the mechanical input which is the mechanical torque and the reference frame, which is in this case the Rotor; have been specified.

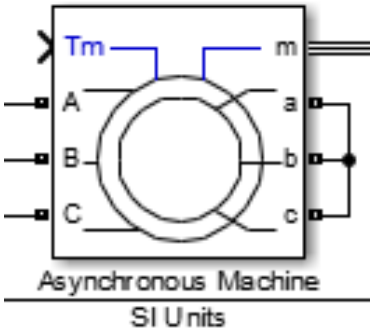

Figure 31. Asynchronous machine block

The Asynchronous machine block implements a three-phase asynchronous machine (wound rotor, single squirrel-cage, or double squirrel-cage). It operates in either generator or motor mode. The mode of operation is dictated by the sign of the mechanical torque: if Tm is positive, the machine acts as a motor, otherwise, the machine acts as a generator. The electrical part of the machine is represented by a fourth-order state-space model, and the mechanical part by a second-order system. All electrical variables and parameters are referred to the stator. All stator and rotor quantities are in the arbitrary two-axis reference frame (dq frame).

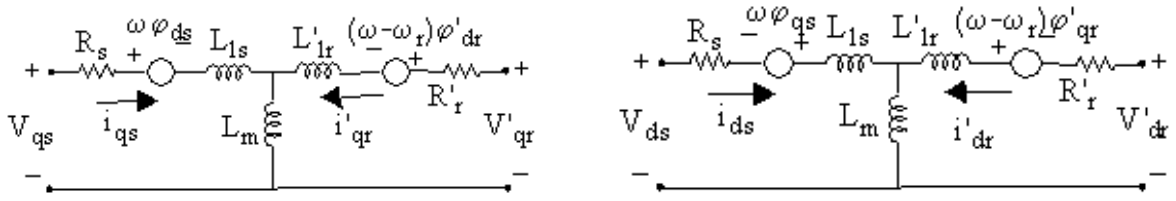

Figure 32. q axis (left) and d axis (right)

$$U_{qst} = R_s \cdot i_{qst} + \frac{\partial \varphi_{qst}}{\partial t} + \omega \cdot \varphi_{dst} \tag{48}$$

$$U_{dst} = R_s \cdot i_{dst} + \frac{\partial \varphi_{dst}}{\partial t} + \omega \cdot \varphi_{qst} \tag{49}$$

$$U'_{qr} = R'_r \cdot i'_{qr} + \frac{\partial \varphi'_{qr}}{\partial t} + (\omega - \omega_r) \cdot \varphi'_{dr} \tag{50}$$

$$U'_{dr} = R'_r \cdot i'_{dr} + \frac{\partial \varphi'_{dr}}{\partial t} + (\omega - \omega_r) \cdot \varphi'_{qr} \tag{51}$$

$$T_{em} = 1,5p(\varphi_{dst} i_{qst} - \varphi_{qst} i_{dst}) \tag{52}$$

Being

$$\varphi_{qst} = L_{st} \cdot i_{qst} + L_m \cdot i'_{qr} \tag{53}$$

$$\varphi_{dst} = L_{st} \cdot i_{dst} + L_m \cdot i'_{dr} \tag{54}$$

$$\varphi'_{qr} = L'_r \cdot i'_{qr} + L_m \cdot i_{qs} \tag{55}$$

$$\varphi'_{dr} = L'_r \cdot i'_{dr} + L_m \cdot i_{ds} \tag{56}$$

$$L_{st} = L_{lst} + L_m \tag{57}$$

$$L'_r = L'_{lr} + L_m \tag{58}$$

Looking at this toolbox, it is clear that the output voltages are short-circuited which means that an squirrel cage motor is being modelled as it is specified at the beginning of section 4.

The output of this Asynchronous toolbox is multiple and then is separated in order to examine each signal in comparison with the result from measurements.

The input voltages in the toolbox (A B C) are the three phase supply voltage which in real motor it comes directly from the network. However, in this simulation a similar behaviour has to be achieved. It is accomplish by means of another toolbox displayed as well in the figure, voltage supply. Inside this toolbox, the following arrangement is what it can be seen.

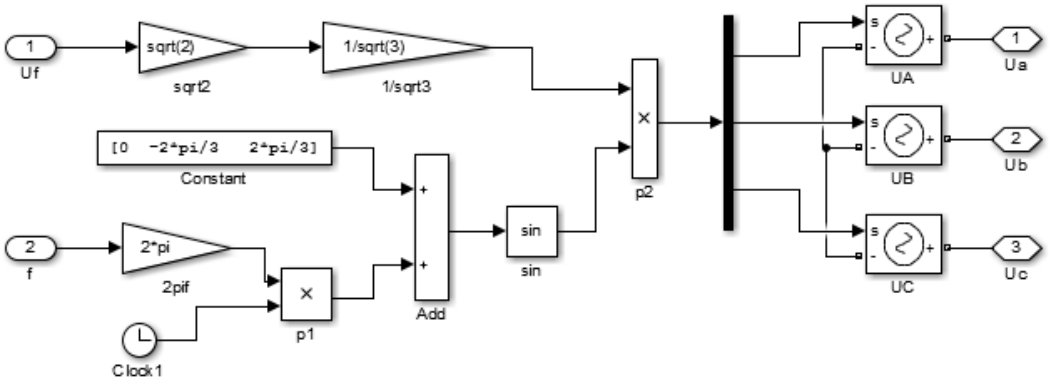

Figure 33. Voltage supply in the mathematical model

Figure 33 shows that voltage supply has been implemented in the model in such a way that it is actually controlled by the voltage measured in order to make it more accurate. Otherwise, it would be controlled by a sinusoidal voltage but without the particular changes in amplitude known by the factual measurements. It is also shown how the three phase voltage are being produced by means of the first toolboxes, after X toolbox the control signal has been achieved and then through the demultiplex the three signals of supply voltage are separated to be the input values for the asynchronous machine.

On the subject of accuracy, it is well known that measurements are more precise than model because they are taken directly from the machine. On the other hand, model does not consider many physical behaviours.

Some simplifications are the following:

- Monoharmonic model only based on one harmonic which is 50 Hz.
- Changes in frequency are neglected. 50 Hz frequency is assumed.
- Thermal effects are not taken into account. As the temperature increases, the value of resistances goes up.
- Not all flux is used, there is always some flux leakage due to slot dispersion.
- Friction on the shaft. It is assumed to be zero.
- Eccentricity in machines. Air-gap does not have the same width in all directions.
- Asymmetry in windings. This happens when we do not have a balanced load, in other words, whether the resistances of the three windings are not equal $R_a \neq R_b \neq R_c$ or the supply is asymmetry $U_a \neq U_b \neq U_c$.
- Torsion. Only one inertia is considered, the inertia of the squirrel cage motor, and there is another machine (DC machine) with another different inertia connected through the shaft.

6 Comparison between model and real motor

In this section two different dynamic states have been analysed through both the measurements in Matlab and the simulation model which has been studied in section 5. To recognize where each data comes from, two different colours have been used: results of measurements are displayed in blue, hence, results from model are in red.

6.1 Start-Up state

In this state, the machine is not working, and later some voltage is supplied leading to the motor start-up. The following graphs show both the measurements and the simulation behaviours. This test has been carried out with the data collected from the reverse start test, only taking into account positive values.

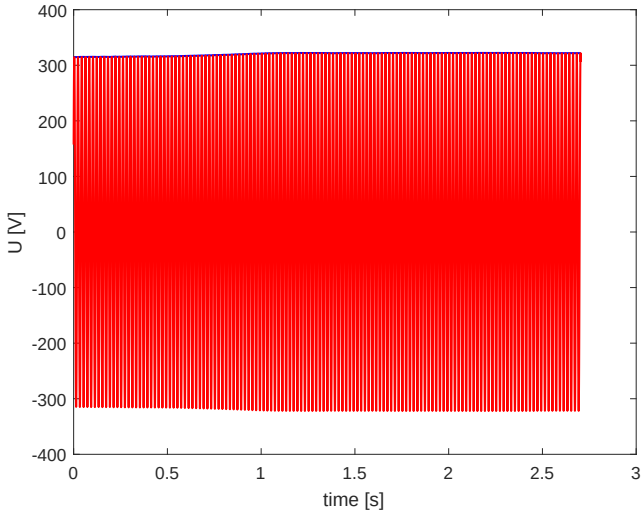

Figure 34. Time domain voltage signal during start-up

From the graph above, it is clear that voltage shift is instantaneous. Once the machine is connected to the network, the voltage is at its stationary position.

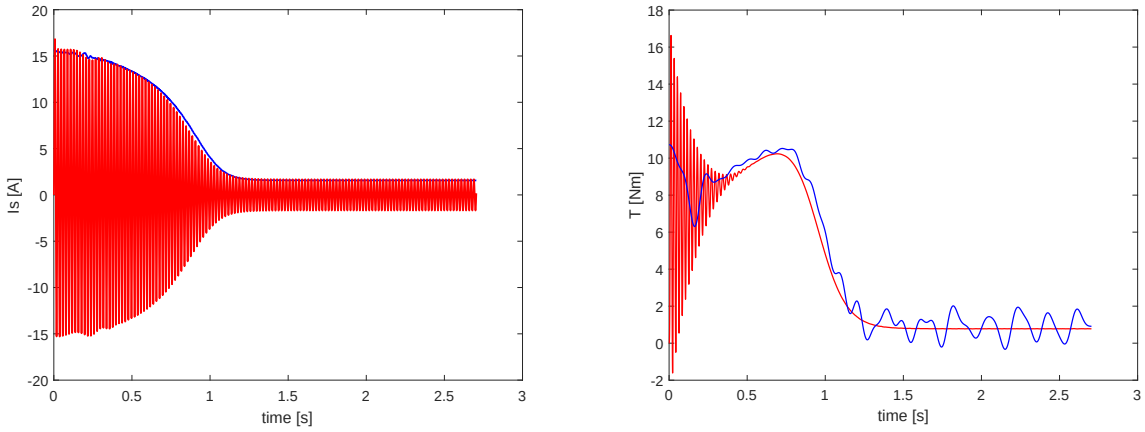

Figure 35. Time domain current signal during start-up (left) and time domain electromagnetic torque signal during start-up (right)

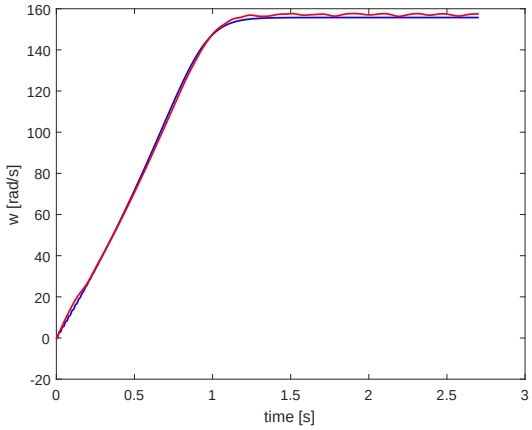

Figure 36. Time domain speed of rotation signal during start-up

The dependence between these graphs has been analysed in section 3. Based on this, it is known that current depends on the slip, therefore, as the rotor speed gets closer to the synchronous, the current goes down, almost reaching zero, due to the low relative speed, or in other words, the low electromagnetic force induced. At the same time, a similar decrease in the electromagnetic torque is produced owing to the decrease in the current flowing.

In view of these graphs, it is noticed that as the speed reaches its steady state, when its value is close to the synchronous, the current and the torque decrease. This can be appreciated around the time 1 s.

From Start-Up graphs, it can be stated that the model chosen is certainly accurate. All peak signal values from model (red) and peak values, which are rms values multiplied by $\sqrt{2}$, from measurements (blue) coincide. In torque graph, during the Start-Up the measurements are nearly the average of model signal.

6.2 Disconnection of three phases

In this dynamic state the motor is working normally and abruptly the three phases of supply voltages are disconnected. The subsequent graphs show both the measurements and the simulation behaviours.

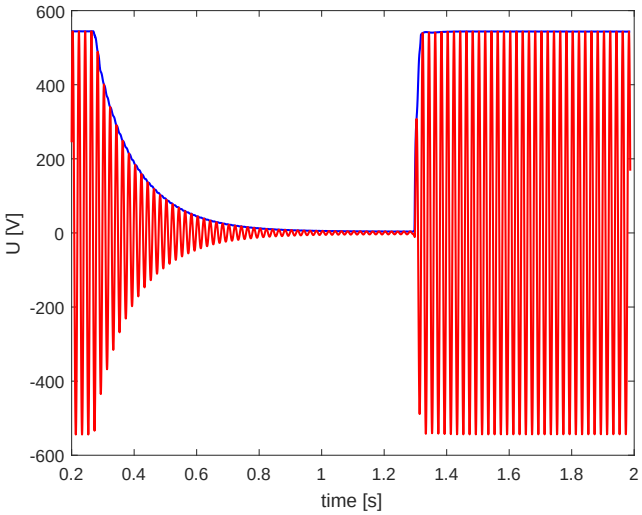

Figure 37. Time domain voltage signal during the disconnection of three phases

Figure 37 shows the decrease in voltage after the disconnection of three phase supply voltage which can be appreciated at the beginning (around 0.25 s). Despite the disconnection is an instantaneous action, voltage does not decrease abruptly due to the remainder voltage induced in the core. Later, at around the time 1.3 s, three phase supply voltage is again connected.

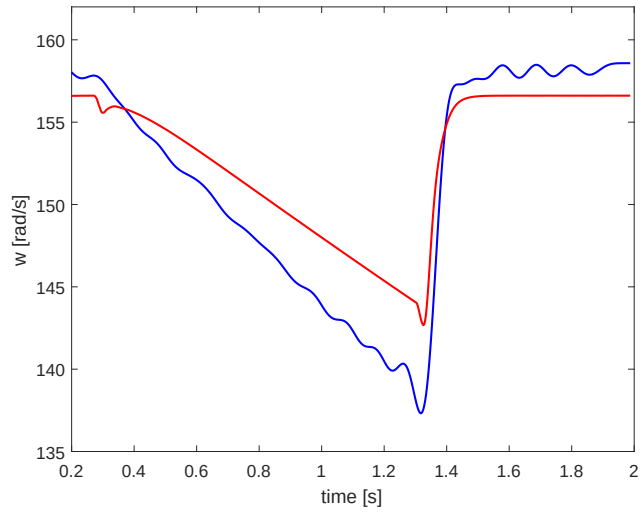

Figure 38. Time domain speed of rotation signal during the disconnection of three phases

Figure 38 displays the effect voltage disconnection has on rotor speed. Once 3 phase supply voltage is disconnected, the rotor speed starts to go down until it stops. However, in this test supply voltage is reconnected at around the time 1.3 s, not leaving the rotor speed reach zero. At the moment of reconnection the rotor is working at approximately 137,5 rad/s based on the measurements, and at 143 rad/s based on the result provided by the model.

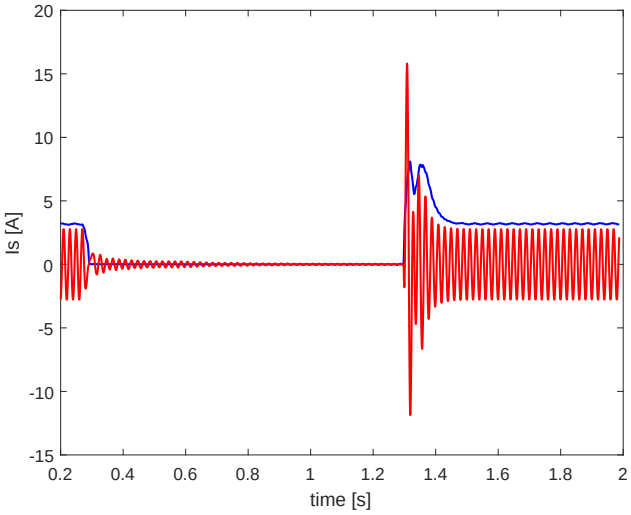

Figure 39. Time domain current signal during the disconnection of three phases

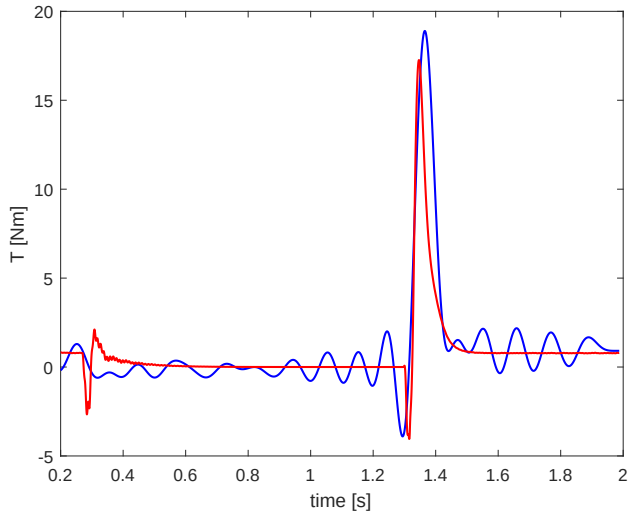

Figure 40. Time domain electromagnetic torque signal during the disconnection of three phases

As it is explained in section 3, the current, and therefore the torque, depends on the slip. From the both graphs above, it is clear that at the moment of disconnection, the rotor speed starts to go down resulting in a decrease in current, and in torque. After approximately 1 s, 3-phase supply voltage is reconnected and the current and torque get higher values during this kind of "Start-Up" and then, they return to their steady states. Is and T behaviours resemble the Start-Up state but with one difference: the rotor speed is not zero during the reconnection, thus, the peak values of current and torque are even lower than the possible ones if it were a real Start-Up.

In view of the previous graphs, the model chosen can be regarded as moderately precise. Voltage graph from both the model and the measurements are exactly the same. On the other hand, speed of rotation is slightly different from one source to another reaching the lower value (approximately 137,5 rad/s) using measurements, an about 143 rad/s by means of the simulation model. For this reason, it can be appreciated that real motor speed decreases quicker than simulation, therefore, it can be stated that inertia value is higher in the model. This difference could be partly due to the simplifications applied to the model. In terms of current and torque graphs, there are slight differences but the results are acceptable.

7 Conclusion

This work has highlighted the relevance of induction machines, devices enhanced over the years due to their reliability and effectiveness. Despite this , as AC-motors, they are more problematic to control by digital methods. To achieve a mathematical model which resembles a real induction motor, it has to be performed taking into consideration all losses, and obviously, the nature of each input value. The one which is implemented in this investigation has been, as it can be seen in section 5.3, monitored by the real supply voltage, which makes the study more reliable.

Based on the comparisons between measurements between real motor and mathematical model in two dynamic states: Start-Up and Disconnection of three phases, it can be stated that the simplifications made in the model do not affect the quality of the solutions. Even many physical issues not being considered, the results are acceptable and in many cases definitely accurate, as it can be appreciated in section 6. For this reason, mathematical models can help in investigation of motor behaviours in any dynamic state and serve as a powerful tool to advance in this area not having the necessity to carry out experiments of different dynamic states with the real motor once its parameters have been calculated through no load, short-circuit, inertia and reverse start tests.

With reference to other possible dynamic states, 1-phase disconnection might be analysed. However, models are not entirely suited to specific cases, and sometimes it is arduous to figure them out. In conclusion, to improve this investigation, other dynamic states should be analysed so that the model may be stated as a precise instrument substitute for real motors taking the advantage of neither time involved nor wear resistance, maintenance, electric spark or even destruction of any part of the machine.

References

[1] W. Jazdzynski: *Nonstationary Models of Induction Motors and their Identification with the Help of Multicriterial Optimisation*. Proceedings of the International Conference on Electrical Machines ICEM96, vol.III, Vigo, Spain, 1996, s.40-45

[2] W. Jazdzynski, W. Milej: *Determining an Improved Dynamic Model of a System: Induction Motor and Direct-Current Machine*. Proceedings of the International Conference on Electrical Machines ICEM 2004, Cracow, Poland, 5-8 September 2004, paper 551, CD-ROM issue.

[3] W. Jazdzynski: *Projektowanie maszyn elektrycznych oraz identyfikacja ich modeli z wykorzystaniem optymalizacji wielokryterialnej*. Wydawnictwa AGH, seria Rozprawy i Monografie nr.28, Krakow 1995.

[4] Victor Giurgiutiu, Sergey Edward Lyshevski: *Micromechatronics Modeling, Analysis and Design with MATLAB*. Second Edition, CRC Press Taylor & Francis Group Boca Raton London New York

[5] Malcolm Barnes: *Practical Variable Speed Drives and Power Electronics*. Elsevier, Oxford, Great Britain, 2003.

[6] Bahram Amin: *Induction Motors Analysis and Torque Control*. Springer, Berlin, Germany, 2001.

[7] Austin Hughes: *ELECTRIC MOTORS AND DRIVES: FUNDAMENTALS, TYPES AND APPLICATIONS*. Second Edition, Newnes,23 November 1993.

[8] Uday A.Bakshi, Mayuresh V.Bakshi: *Transformers & Induction Machines*. Technical Publications Pune, First Edition, India, 2008.

[9] Construction of 3-Phase AC induction motors, [date of access: 20.05.2016], http://electrical-engineering-portal.com/construction-of-3-phase-ac-induction-motors

[10] Construction of Three Phase Induction Motor, [date of access: 20.05.2016], http://www.electrical4u.com/construction-of-three-phase-induction-motor/

[11] Armature Winding — Pole Pitch Coil Span Commutator Pitch, [date of access: 21.05.2016], http://www.electrical4u.com/armature-winding-pole-pitch-coil-span-commutator-pitch/

[12] How are Squirrel Cage Induction Motors Constructed?, [date of access: 22.05.2016],http://www.brighthubengineering.com/diy-electronics-devices/43723-how-are-squirrel-cage-induction-motors-constructed/

[13] Double Squirrel Cage Motor, [date of access: 25.05.2016], http://www.electricaleasy.com/2014/02/double-squirrel-cage-motor.html

[14] Deep Bar Rotors in Induction Machines, [date of access: 25.05.2016], http://www.electrotechnik.net/2015/05/deep-bar-rotors-in-induction-motors.html

[15] Deep Bar Double Cage Induction Motor, [date of access: 25.05.2016], http://www.electrical4u.com/ deep-bar-double-cage-induction-motor/

[16] C-IM1-4 Temat: Dynamika maszyny indukcyjnej, [date of access: 6.06.2016], http://www.keiaspe.agh.edu.pl/keiaspe/articles/0100/5013/IM1-IM4_instrukcja_i_materialy2.pdf

[17] Simulacion de la Maquina de Induccion en un eje de referencia arbitrario qd0, [date of access: 8.06.2016], http://sisbib.unmsm.edu.pe/bibvirtualdata/publicaciones/electronica/Agosto_2000/pdf/simulacion.pdf

[18] Entendiendo la Transformacion de Park, [date of access: 6.06.2016], http://fglongatt.org/OLD/Reportes/RPT2004-01.pdf

[19] Induction Motor Modelling for Vector Control Purposes, [date of access: 8.06.2016], http://www.motor-design.com/cmsAdmin/uploads/induction_motor_modelling.pdf

[20] A comparative study between Vector Control and Direct Torque Control of Induction Motor using MATLAB SIMULINK, [date of access: 8.06.2016], http:/digitool.library.colostate.edu/webclient/DeliveryManager/digitool_items/csu01_storage/2013/03/01/file_1/186695

[21] Induction Motor, [date of access: 17.05.2016], https://en.wikipedia.org/wiki/Induction_motor

[22] Teslas AC Induction Motor is one of the greatest discoveries of all time, [date of access: 2.06.2016], http://www.teslasociety.com/hall_of_fame.htm

[23] The invention of the electric motor 1856-1893, [date of access: 26.05.2016], https://www.eti.kit.edu/english/1390.php

[24] Future Adjustable Speed Motor Technology - Issue 10, 2008, [date of access: 28.06.2016], http://library.automationdirect.com/future-adjustable-speed-motor-technology-issue-10-2008/

[25] Squirrel-cage rotor, [date of access: 23.05.2016], https://en.wikipedia.org/wiki/Squirrel-cage_rotor

[26] Motors, efficiency, and adjustable-speed drives, [date of access: 3.07.2016], http://powerelectronics.com/motion-systems/motors-efficiency-and-adjustable-speed-drives

[27] Production of rotating magnetic field in polyphase stator, [date of access: 2.07.2016], http://www.electricaleasy.com/2014/02/production-of-rotating-magnetic-field.html

[28] Chapter 3: AC and DC Motors - AC Motors: Control of speed, Torque and Horsepower, [date of access: 2.07.2016], http://www.globalspec.com/reference/10795/179909/chapter-3-ac-and-dc-motors-ac-motors-control-of-speed-torque-and-horsepower

[29] Tesla Polyphase Induction Motors, Chapter 13 - AC Motors, [date of access: 29.05.2016], http://www.allaboutcircuits.com/textbook/alternating-current/chpt-13/tesla-polyphase-induction-motors/

[30] Application basics of operation of three-phase induction motors, [date of access: 3.07.2016], https://www.rockwellautomation.com/resources/downloads/rockwellautomation/che /pdf/Application_basics_operation_three_phase_induction_motors.pdf

[31] AGH EAIiIB DYNAMIKA SYSTEMOW ELEKTROMECHANICZNYCH Rok I, II stopie stacjonarne, rok akademicki: 2012/2013 Kierunek: Elektrotechnika, Specjalno sc: , [date of access: 7.06.2016], http://www.keiaspe.agh.edu.pl/keiaspe/articles/0100/5013/IM1-IM4_Formatka.pdf

[32] Slip Ring Induction Motors Basics, [date of access: 3.07.2016], http://www.brighthubengineering.com/diy-electronics-devices/43725-slip-ring-induction-motors-basics/